IPPT Reports on Fundamental Technological Research
2/2016

Krzysztof Zembrzycki, Sylwia Pawłowska
Paweł Nakielski, Filippo Pierini

DEVELOPMENT OF A HYBRID ATOMIC FORCE MICROSCOPE AND OPTICAL TWEEZERS APPARATUS

Institute of Fundamental Technological Research
Polish Academy of Sciences

Warsaw 2016

IPPT Reports on Fundamental Technological Research

ISSN 2299-3657
ISBN 978-83-89687-99-9

Received on 8th April 2016

Institute of Fundamental Technological Research Polish Academy of Sciences
Instytut Podstawowych Problemów Techniki Polskiej Akademii Nauk (IPPT-PAN)
Pawińskiego 5B, PL 02-106 Warsaw, Poland

Printed by/Druk:
Drukarnia Braci Grodzickich, Piaseczno, ul. Geodetów 47A

Acknowledgements

This work was supported by NCN grant
no. 2011/03/B/ST8/05481.
Research subject carried out with the use of CePT infrastructure
financed by the European Union –
the European Regional Development Fund within
the Operational Program “Innovative Economy” for 2007–2013.
The authors gratefully acknowledge NT-MDT
for technical support.
In addition, we would like to thank IOP Publishing to provide us
with the permission to reproduce part of the paper: “Atomic force
microscopy combined with optical tweezers (AFM/OT)” [1].

Development of a hybrid Atomic Force Microscope and Optical Tweezers apparatus

Krzysztof Zembrzycki, Sylwia Pawłowska
Paweł Nakielski, Filippo Pierini

Institute of Fundamental Technological Research
Polish Academy of Sciences

Abstract

The role of mechanical properties is essential to understand molecular, biological materials and nanostructures dynamics and interaction processes. Atomic force microscopy (AFM), due to its sensitivity is the most commonly used method of direct force evaluation. Yet because of its technical limitations this single probe technique is unable to detect forces with femtonewton resolution. In this paper, we present the development of a combined atomic force microscopy and optical tweezers (AFM/OT) instrument. The system is based on a commercial AFM and confocal microscope. The addition of three lasers along with beam shaping and steering optics, on which the optical tweezer is based upon, provide us with the ability to manipulate small dielectric objects suspended in a fluid. Additionally, this same device allows for direct displacement and force measurement with very high resolution and accuracy in the same AFM scanning zone. We have also fitted a laser and a set of filters to observe fluorescent samples appropriately exited. We show that this is a great improvement of a standalone AFM force resolution and more so opens a way to conduct experiments using a hybrid double probe technique with high potential in nanomechanics, molecules manipulation and biological studies. This paper describes in detail the construction of all the modules such as the trapping laser optics, detection laser optics and the fluorescence module. Also, due to its importance on the performance of the equipment, the electronics part of the detection system is described. In the following chapters the whole adjustment and calibration is explained. The performance of the apparatus is fully characterized by studying the ability to trap dielectric objects and quantifying the detectable and applicable forces. The setting and sensitivity of the particle position detector and force sensor is shown. We additionally describe and compare different optical tweezer calibration methods. In the last part we show the ability of our instrument to conduct experiments using the proposed double-probe technique, in this case to study interaction forces between two particles.

Development of a hybrid Atomic Force Microscope and Optical Tweezers apparatus

Krzysztof Zembrzycki, Sylwia Pawłowska
Paweł Nakielski, Filippo Pierini

Instytut Podstawowych Problemów Techniki
Polskiej Akademii Nauk

Abstrakt

Pomiary własności mechanicznych i sił w mikro- i nanoskali mają bardzo ważne znaczenie w badaniach dynamiki i oddziaływań materiałów biologicznych i nanostruktur. Mikroskopia sił atomowych (ang. AFM), z uwagi na swoją czułość, jest najczęściej używaną techniką do bezpośredniego pomiaru sił. Jednak z powodu swoich ograniczeń nie jest w stanie mierzyć sił w zakresie femtonewtonów z odpowiednią rozdzielczością. Takie możliwości stwarza metoda optyczna oparta na tzw. szczypcach optycznych (ang. OT). Z drugiej strony, z uwagi na fizyczne ograniczenia tej metody, pomiary charakteryzujące powierzchnie oddziaływujące w niewielkich odległościach, nadal wymagają stosowania mikroskopii sił atomowych. W naszej pracy opisujemy unikalną konstrukcję hybrydową opartą na połączeniu obu technik w jednym systemie. Stworzony system AFM/OT pozwala na bezpośrednie pomiary przemieszczenia oraz siły z bardzo dużą rozdzielczością i dokładnością w obszarze działania sondy AFM. Dodatkowo system został wyposażony w elementy optyczne pozwalające na pobudzanie i detekcję fluorescencji. Wykazujemy, że ten instrument istotnie poprawia zakres i rozdzielczość sił mierzonych za pomocą standardowego mikroskopu AFM, jak również otwiera drogę do prowadzenia eksperymentów z użyciem hybrydowej techniki dwóch sond, mającej wysoki potencjał zastosowań w nanomechanice, badaniach biologicznych i nanomanipulacji.

Praca przedstawia szczegóły konstrukcyjne zbudowanych modułów szczypiec optycznych, jak i układ elektroniczny pozwalający na precyzyjne pomiary przemieszczeń obiektów uwięzionych przez szczypce optyczne. W kolejnych rozdziałach jest przedstawiona procedura dostrajania układu optycznego i metodyka kalibracji. W ostatniej części przedstawiamy, na przykładzie pomiaru oddziaływań bliskiego kontaktu dwóch cząstek koloidalnych, potencjał naszego instrumentu do prowadzenia pomiarów z jednoczesnym użyciem techniki dwóch sond (AFM/OT).

Contents

1

Introduction

Force has a crucial role in physical, chemical and biological processes. The knowledge of mechanical forces involved in single molecules, nanomaterials and biological objects activities is fundamental in understanding their structure, function and behaviour. The study of forces involved in molecular and nanomaterial interactions represents one of the most interesting contemporary challenges. Several techniques have been recently used to measure directly the forces required to unbind molecules, the surface forces responsible for nanoparticle stability, and to quantify mechanical properties of biological tissues and cells. Over the last few decades atomic force microscopy (AFM) has been the technique most frequently used to measure interaction forces of molecules and nanomaterials [2]. AFM is an evolution of scanning tunnelling microscope (STM) that immediately gained popularity thanks to its ability to analyse soft and electrically non-conductive material [3]. Initially, AFM was developed for nanoscale imaging purposes, where a topographical reconstruction is obtained by scanning the sample surface using a tip fixed on a flexible cantilever. The spatial resolution has been enhanced using very sharp probes. Over the years, numerous implementations have been proposed which have allowed this equipment to cover a broad range of applications starting from electrical to force measurements. Thanks to the technical development of AFM instrumentation, such as the introduction of the piezo stage and microfabricated cantilevers, remarkable improvements in force measurements have been achieved [4, 5]. On the other hand, atomic force microscopy has limited use for examining small forces because its sensitivity is strictly dependent on the laser beam properties and the mechanical property of the probe [6]. The background noise of AFM arises from a number of environmental and instrumental factors, mainly from the intensity and shape of the laser beam incident on the surface of the probe and the thermal excitation of the cantilever and it cannot be totally removed. If a soft cantilever with small spring constants in the range of 0.1–0.01 N/m is used, the typical detectable force range is between 10 piconewton (pN) and 10^4 pN, with a spatial and temporal resolution from 0.5 nanometer (nm) to 1 nm and 10^{-3} s respective-

ly [7]. Due to these technical limitations, AFM is of limited usefulness in the study of the dynamic of processes in which very low forces are involved (typically on the order of few femtonewtons).

Over the years many techniques have been developed in order to manipulate micro-objects suspended in water, such as magnetic and ultrasound traps. Unfortunately most of them have very limited usage due to their experimental limitations, like the necessity to use specific materials for magnetic traps to work. Among of many ideas, Optical Tweezers (OT) stand out for their high resolution and flexibility [7]. Optical tweezers are a technique capable of trapping small particles using the forces generated by laser radiation pressure. The concept of pressure from the propagation of light is at the core of optical tweezer's technology and was hypothesized several centuries ago. Until the 1960s it was not possible to use radiation pressure generated by light in order to modify the position of matter, but in those years the advent of lasers provided a light source with the appropriate properties to generate a light trap and the rise of nanotechnology gave the opportunity to synthesize, modify and control materials in the nanometric scale. These two factors opened the way for optical trapping. Arthur Ashkin is the developer of ‘single-beam gradient force trap’, the technique that we now call optical tweezers [8]. In the 1970s Ashkin studied interactions between micromaterials and light and he was able to trap particles in a confined three-dimensional space using the forces of light radiation. In the following years, Ashkin was able to demonstrate that it is possible to apply forces in the piconewton scale on small dielectric microspheres by focused laser beams using a high numerical aperture microscope objective [9]. Today Optical traps can be used to manipulate and study not only dielectric spheres with dimensions in the micron range, but also metal particles and single molecules in the range of nanometers. Additionally, the shape and polarisation of the trapping potential can be modified to match the needs of a specific experiment [10].

1.1. Theoretical background

The force on a dielectric particle is strictly related to the change in light momentum due to the refraction of light by the object, so light can exert a force on all objects that refracts or reflects the beam [9]. Due to the nature of optical rays, there are a multitude of forces involved in the system that result from multiple reflections and refractions of optical beams from the surface of the trapped object.

For stable trapping in all three dimensions, the axial gradient component of the force pulling the particle towards the focal region must exceed the scattering component of the force pushing it away from that region. This condition necessitates a large steep gradient of light intensity, produced by a trapping laser beam sharply focused to a diffraction-limited spot using an objective of high NA. As a result of this balance between the gradient force and the scattering force, the axial equilibrium position of a trapped particle is located slightly beyond the focal point. For small displacements (~150 nm), the gradient restoring force is simply proportional to the offset from the equilibrium position (i.e., the optical trap acts as Hookean spring whose characteristic stiffness is proportional to the light intensity) [11].

One of the fundamental requirements of this system is the use of particles having a higher index of refraction than their neighbouring medium. The index of refraction ratios (η_p/η_w) should be higher than 1.1. According to Snell's law, when the light coming from a medium passes into a dielectric material with low refractive index the rays are deflected.

The typical optical tweezers configuration where a focused laser beam passes through a polystyrene microparticle with higher diameter than the incident light wavelength ($a > \lambda$) is schematized in Fig. 1.1.

The particle behaves as a convergent lens refracting the light and the ray optics treatment can be used to explain the nature of forces involved in the trapping. The force due to the scattering pushes the bead in the same direction as the light propagation, the gradient forces due to the refraction pull the bead in the opposite direction. Because of the refraction and the scattering of the rays the polystyrene bead is attracted to the point where the light is focused. If an external force pushes the particle away from the centre of the trap, the refracted light path changes and the gradient force, due to the change of the momentum, replaces the sphere into the initial position. The system achieves a stable condition when the gradient force is large enough to overcome the scattering force and when the total energy involved in the trapping process is bigger than the thermal energy of the trapped object [12].

When the trapped sphere is much smaller than the wavelength of the trapping laser, i.e., $a \ll \lambda$, the conditions for Rayleigh scattering are satisfied and optical forces can be calculated by treating the particle as a point dipole. In this approximation, the scattering and gradient force components are readily separated. The scattering force is due to absorption and reradiation of light by the dipole. For a sphere of radius a, this force is [11]:

$$F_{\text{scatt}} = \frac{I_0 \sigma n_m}{c}, \tag{1.1}$$

$$\sigma = \frac{128\pi^5 a^6}{3\lambda^4}\left(\frac{m^2-1}{m^2+2}\right), \tag{1.2}$$

$$m = \frac{n_p}{n_m}, \tag{1.3}$$

where I_0 is the intensity of the incident light, σ is the scattering cross section of the sphere, n_m is the index of refraction of the medium, n_p is the index of refraction of the particle, c is the speed of light in vacuum and λ is the wavelength of the trapping laser.

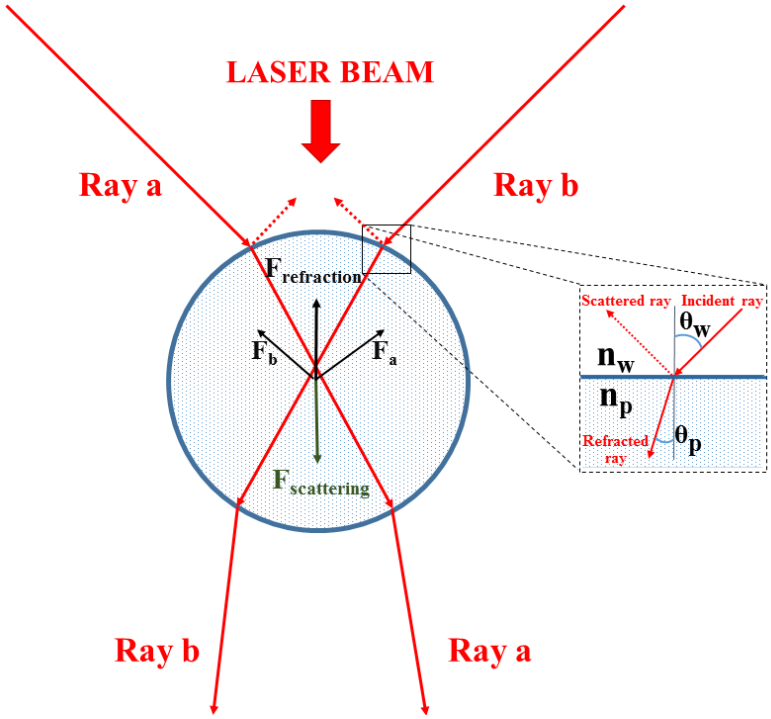

Figure 1.1. Schematic diagram showing the optical tweezers ray optics model. A transparent polystyrene microparticle is illuminated by a focused Gaussian laser beam. The forces on the dielectric spherical bead due to scattering and refraction of light rays are balanced. Inset is a graphical representation of the influence of the index of refraction in the deflection of rays at the water-particle interface and the splitting of incident ray in two component: scattered ray and refracted ray.

The scattering force is in the direction of propagation of the incident light and is proportional the intensity. The time-averaged gradient force arises from the interaction of the induced dipole with the inhomogeneous electromagnetic field:

$$F_{\text{grad}} = \frac{2\pi\alpha}{\text{cn}_m^2}\nabla I_0, \tag{1.4}$$

where

$$\alpha = \text{n}_m^2 a^3 \left(\frac{m^2-1}{m^2+2}\right), \tag{1.5}$$

is the polarizability of the sphere. The gradient force is proportional to the intensity gradient, and points up the gradient when $m > 1$. When the dimensions of the trapped particle are comparable to the wavelength of the trapping laser ($a \sim \lambda$), neither the ray optic nor the point-dipole approach is valid. Instead, more complete electromagnetic theories are required to supply an accurate description. Unfortunately, the majority of objects that are useful or interesting to trap, in practice, tend to fall into this intermediate size range (0.1–10 λ). As a practical matter, it can be difficult to work with objects smaller than can be readily observed by video microscopy (~0.1 μm), although particles as small as ~35 nm in diameter have been successfully trapped. Dielectric microspheres used alone or as handles to manipulate other objects are typically in the range of ~0.2–5 μm [11].

The trap force applied by the optical tweezers to the trapped particle behaves as a harmonic spring and can be described by the following equation:

$$F = kx, \tag{1.6}$$

where F is the applied force, x is the particle displacement from the centre of the trap and k is the spring constant. In order to use optical tweezers as a quantitative force sensor it is necessary to calibrate the trap stiffness measuring the displacement of a sphere in the trap when known external forces are applied to the particle [13].

The ability to manipulate single molecules, attached to trapped micro or nanoparticles, with high resolution and to measure forces with femtonewton accuracy opened the way to the study of several important new topics using optical tweezers [14–16].

Biologists were able to take immediate advantage of optical tweezers using this apparatus as a tool to study several biological systems and single molecules [17, 18]. Optical tweezers have been used for single molecule studies of biopolymers, where

single molecules of DNA, RNA or proteins have been twisted, stretched [19] and unfolded to measure its mechanical properties [20]. The ability to measure forces at low scale has also been used in the study of the kinetics of motor proteins like RNA polymerase, myosin and kinesin [16, 19]. Optical tweezers have been used in studying intracellular organelles' movement [21], in cell sorting [22] and flow virometry [23].

Over the years the use of optical tweezers has been opening new perspectives in several branches of physics. Optical tweezers have been used to study the movement of micro and nanoparticles in colloidal systems at different time scales starting from Brownian to ballistic motion [24] and the rotation of non-symmetric objects [25]. Optical trap can also be used to calculate the impact of surface modification on surface forces and drag coefficients of nanoparticles [26], to study rheology [27, 28] and the forces involved in single particle collisions and aggregation [29].

The aim of the present work is to demonstrate the possibility of extending the capability of a commercial AFM system by combining it with optical tweezers. It permits obtaining a high-quality imaging instrument able to trap and modify nanometric materials and to measure force in the subpiconewton scale. In this perspective, we have designed, built and calibrated an integrated AFM-optical tweezers apparatus. An exhaustive description of the AFM-optical tweezers setup is given in this article. We proved the instrument performance that allows us to manipulate single polystyrene particles. We analysed the quadrant photodiode detector noise and its response to the displacement of a particle from the centre of the trap. The movement of the piezo stage was used to measure the optical tweezer's behaviour and to calculate trapping force using the drag-force calibration method. The calibration procedure was confirmed by comparing the previously obtained results, from the external force calibration, with those achieved using the equipartition method. The knowledge of optical trap stiffness is fundamental in single molecules, biological and single colloidal object studies to provide a comprehensive quantitative value of the forces involved in molecules and nanomaterials interactions.

2

Experimental setup

2.1. Optical Tweezers setup

A hybrid AFM/Optical Tweezers apparatus, capable of trapping a single micrometric object and to measure forces with femtonewton resolution was built. The experimental setup is shown in Figs. 2.1 and 2.2. Our optical tweezers instrument is based on the inverted microscope (IX71, Olympus Optical Co. Ltd, Tokyo, Japan) of an AFM system (Ntegra Spectra, NT-MDT, Limerick, Ireland). The system uses three different lasers, each preforming a different task. A 1064 nm Nd:YAG diode pumped solid state laser, with a maximum output power of 2 W (Cobolt Rumba CW 1064 nm DPSSL, Cobolt, Solna, Sweden) along with beam condiditoning elements, is employed to create an optical trap that could confine single objects in colloidal systems. Several factors contributed to the choice of trapping laser wavelength. Usually, biological matter like living cells has relative transparency in the near infrared region. Biological chromospheres absorb increasingly less light in the infrared range and water absorbs more strongly at the highest value of wavelength ($\lambda > 2000$ nm). Studies on cells have shown that the interaction with a laser beam in the range of wavelengths of 800 nm to 1100 nm does not affect cell growth [30]. Hence, a Nd:YAG laser source, able to generate a 1064 nm wavelength Gaussian beam, was chosen because it provides the suitable power, wavelength and profile to trap colloidal particles and biological material avoiding heat-related damage.

The second, a 633 nm He-Ne laser (25 LHP 991, Melles Griot, Irvine, California, USA) is the core of our most sensitive detection system. This type of laser was chosen for its superior beam quality and low noise, which are essential in order to achieve high spatial and temporal resolutions of the object position within the optical trap. The purpose for not using the trapping laser for this purpose is to make the detection system independent of the trap settings. Due to the nature of the signal converters, such as photodiodes and transimpedance amplifiers, the signal to noise ratio (SNR) will in

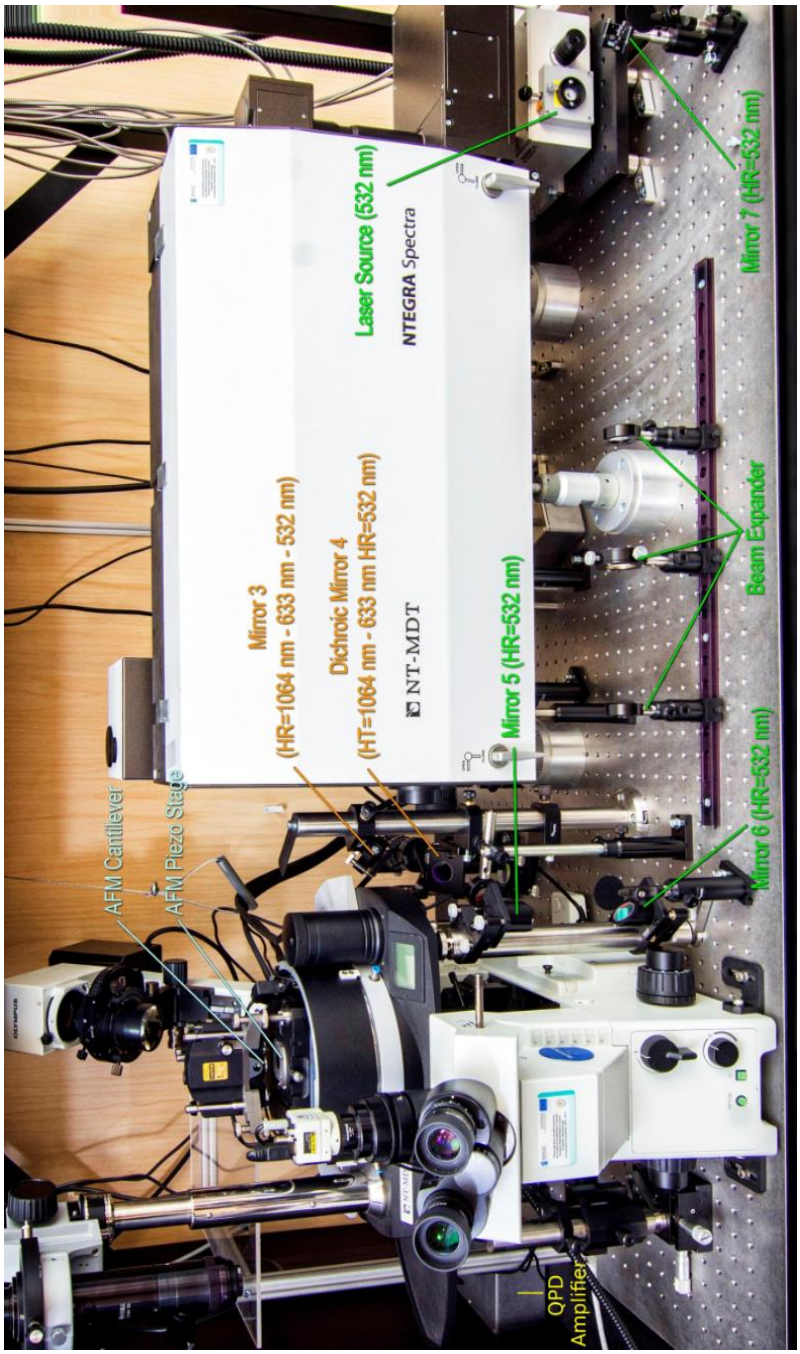

Figure 2.1. Picture of the front side of our hybrid AFM-optical tweezers station built around an inverted microscope and an atomic force microscope. The system uses three lasers with wavelengths of 532 nm, 633 nm and 1064 nm each adjusted to the sample plane. The big white chassis in the middle of the image is the confocal and Raman spectrometer module and is not relevant to the optical tweezers.

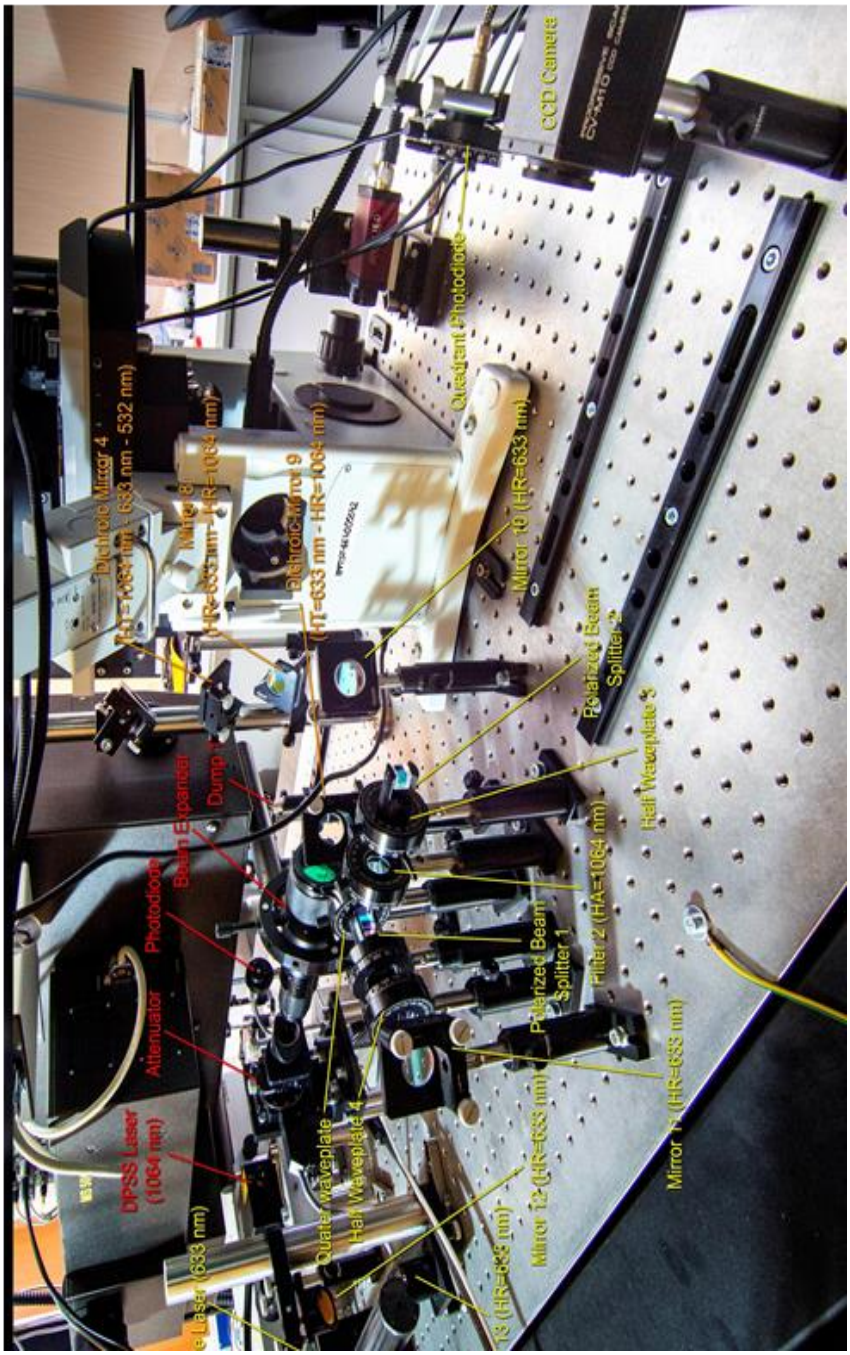

Figure 2.2. Picture of the back side of our hybrid AFM/OT. In the center the back side of the Olympus microscope, in the upper left the back side of the confocal module. All the elements of the OT are placed on the optical table.

part depend on the amount of light that is reflected from the trapped particle. Therefore, if the same laser source was used for both trapping and detection, the SNR would additionally be a function of the trapping laser power, or the trap stiffness. This would not only make the data analysis and error assessment unnecessary difficult, but also degrade the detection system performance at very low and very high trap powers due to low SNR and limitations of the photodetectors both dynamic range and linearity.

The third a 532 nm wavelength pulsed laser (NL202, Ekspla, Vilnius, Lithuania) is used to excite fluorescent materials for imaging purposes. It has a maximum pulse frequency of 1 kHz. This particular wavelength was chosen because many fluorescent dyes, such as fluorescein or JOJO-1 that are frequently used to tag microparticles or biological materials such as DNA, have their absorption maximum close to the 532 nm wavelength.

The base of our optical tweezers is an inverted optical microscope which is part of a commercial atomic force microscope. This set-up allows us to combine optical tweezers with AFM. The AFM piezo stage controlled by a computer gives the opportunity to displace the trapped particle and to control sample position with subnanometer accuracy. In order to decrease mechanical perturbations the instrument is mounted on an optical table with both passive and active vibration isolation. A computer is used to control the piezo stage movements, the light power and to collect and analyze numerical data.

The base of the instrument is an inverted optical microscope (Fig. 2.3). Mounted to it is the precision piezo-stage which can move the sample in X and Y directions (which are perpendicular to each other and the optical axis), and from the bottom the oil-immersion objective (UPlanFl, Olympus Optical Co. Ltd, Tokyo, Japan) which has 100x magnification and a numerical aperture of 1.30 and can be moved along the Z axis. Above the sample there is place for the AFM head and light source. All the lasers employed in this apparatus, 532 nm (Laser Source 1), 633 nm (Laser Source 3) and 1064 nm (Laser Source 2) must have individually set beam parameters, such as diameter, polarization, divergence, and must enter the microscope objective while sharing its optical axis. The Dichroic Mirror 1 couples the three laser paths from the main periscope to that axis. Also, on the microscope there is an intensified high speed camera (HiCAM 500; Lambert Instruments, Leutingewolde, The Netherlands), that is used for visualization of the trapped objects and their surrounding in both white and fluorescent light. The Filter 1 placed before the camera cuts off any back scattered light from all the lasers that would normally swamp the camera with noise.

The laser paths use several mirrors and a periscope to direct the beam into the microscope (Fig. 2.4). The Dichroic Mirror 4, in the main periscope, is used to couple

the fluorescent laser light in the optical axis of the trapping and detection lasers. Beam Expander 1 provides a suitable excitation beam shape in order to have equal power density in the whole aperture in the focus plane of the objective.

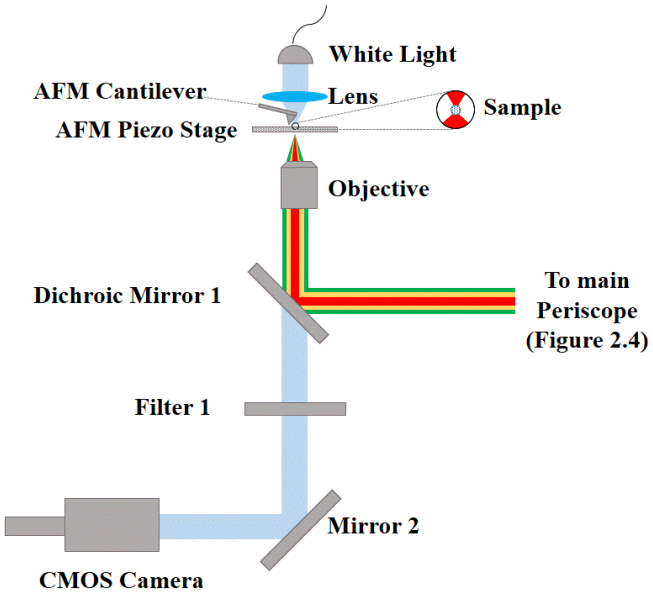

Figure 2.3. Basic elements of the microscope. The Dichroic Mirror 1 is used to couple all the lasers of the trap to the optical axis of the microscope and the objective itself. The Filter 1 is used to filter out the remnants of the scattered lasers light from the camera image.

The beam of the main trapping laser (Laser Source 2) has to be modified in order to have an appropriate shape and power to form a stable and adjustable trap (Fig. 2.5). Additionally, its power output has to be monitored in the course of the experiment. The laser head is mounted on a water cooled heat sink with temperature stabilization in order to eliminate any heat related drift. Forced air cooling is not advisable since fans produce a lot of vibrations that get coupled to the optical table and thus in the whole device. The Half-Wave Plate 1 is mounted on a motorized rotation stage and along with Polarizer 1 acts as an adjustable power regulator. The excess laser power is reflected in to a beam Dump 1. Additionally, part of that power is reflected by a Glass Plate on to a Photodiode that provides a feedback system to monitor the output power of the attenuator. The part of the laser power that passes through the polarizer gets expanded by Beam Expander 2 in order to form a beam diameter that will overfill

the back aperture of the objective. After that it gets coupled in to the beam path of the detection laser by Dichroic Mirror 9.

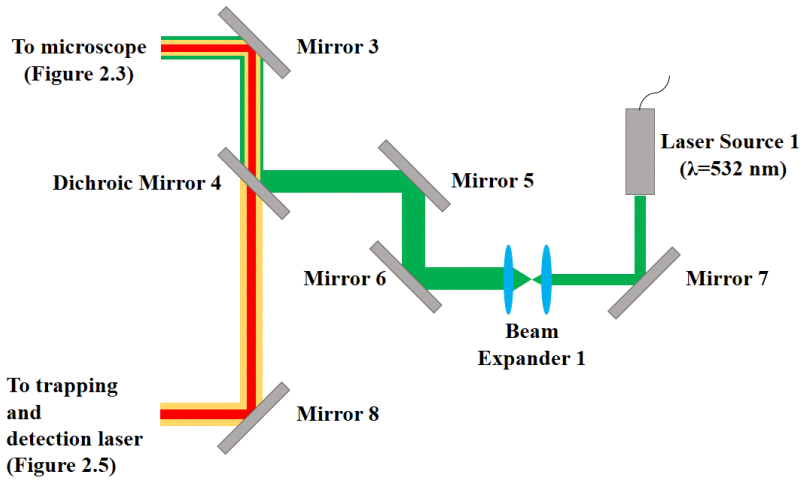

Figure 2.4. Main periscope. It is used to direct the lasers to the optical microscope. Dichroic Mirror 4 is used to couple the 532 nm fluorescence excitation laser to the main optical path of the OT. Mirror 5 and 6, make a secondary periscope.

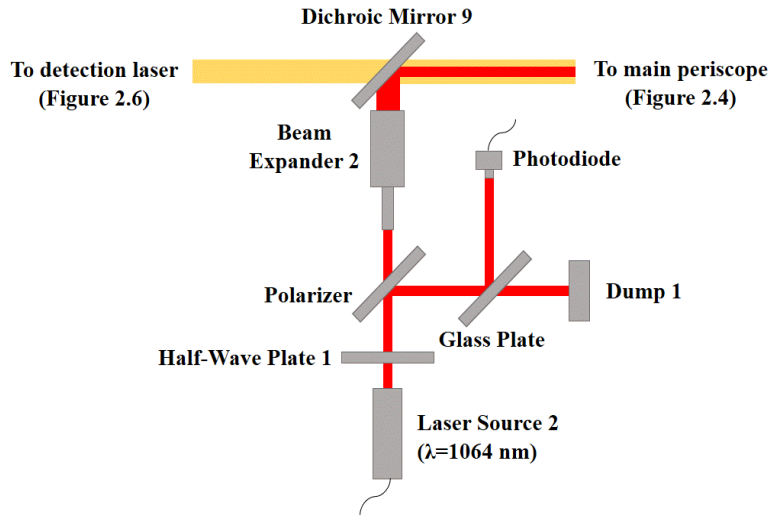

Figure 2.5. Trapping laser conditioning and coupling. The Half-Wave Plate 1 is mounted on a motorized rotating stage and can be controlled by the computer.

The detection of the particles position within the trap is performed by imaging, on to a quadrant photodiode, the diffraction pattern of the detection laser light backscattered form that particle (Fig. 2.6). This kind of configuration is much more complicated that the more common one, in which the laser light is gathered by a condenser, yet this is compensated by the fact that the space on the other side of the sample is free. This allows for the AFM head to be placed on the upper side of the sample and thus enable us to use both techniques at the same time. The beam of Laser Source 3 is

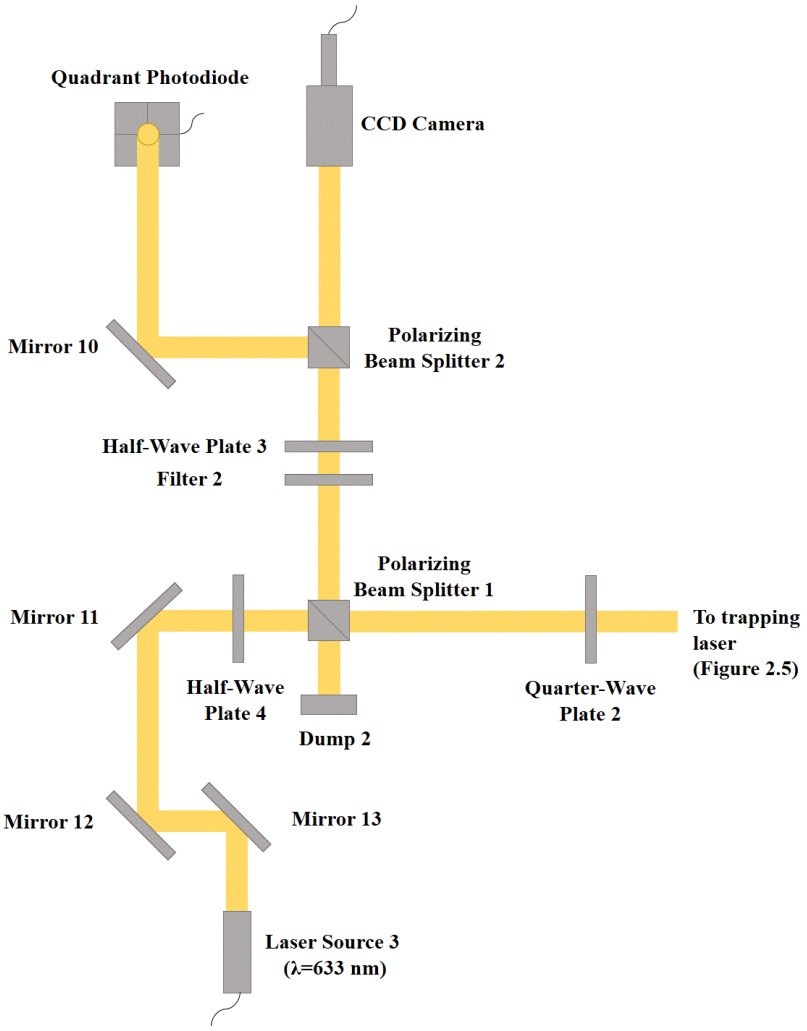

Figure 2.6. Schematic of the detection laser path.

directed to the main optical axis, and passes through the Half-Wave Plate 4 which acts as a power regulator along with Polarizing Beam Splitter 1. Then the linear laser polarization get converted to a circular polarization by the Quarter-Wave Plate 2 and travels along the main optical axis to the objective and the sample. There on the trapped object it gets reflected and travels back along the same optical path, but now with an opposite rotation of its polarization vector. When its goes through the Quarter-Wave Plate 2, it get converted back to a linear polarized light but with a 90^{O} shift and thus gets reflected by Polarizing Beam Splitter 1 on to the optical part responsible for the detection. Filter 2 cuts out any possible remnants of the trapping laser light. A CCD camera (CV-M10 RS, JAI, Yokohama, Japan) is used to image the interference pattern which helps in adjustments and in validation if a correct object was trapped (e.g. it is very easy to distinguish when a single particle is trapped or more than one just by looking at the pattern shape, while it is not so obvious on the microscope image with fluorescent or white light illumination). The main position detector is a Quadrant Photodiode (QPD, S4349, Hamamatsu Photonics Inc., Hamamatsu, Japan). The division of light power between the camera and the QPD is done by Half-Wave Plate 3 and Polarizing Beam Splitter 2.

The quantitative position and force analysis were carried out by measuring the shift of the backscattered light by the quadrant photodiode (Fig. 2.7). The detector is made up of four identical photodiodes arranged in a quadrant array. Every quadrant behaves like a single photodiode and generates an electrical current proportional to

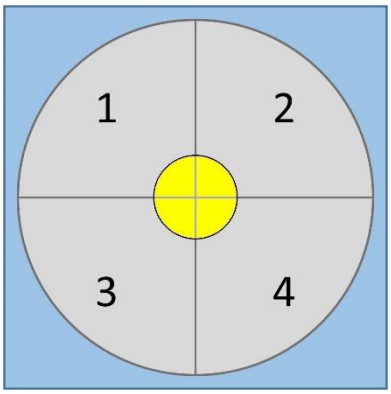

Figure 2.7. Schematic diagram of a quadrant photodiode. The detector surface is divided in four independent quadrants that generate four electrical signals. The yellow circle represents the incident backscattered light beam. The produced signals voltage depends on the quantity of collected light. For a particle perfectly centered in the trap, the resulting backscattered beam is directed to the middle of the quadrant photodiode.

the intensity of light induced on it. A specially built amplifier converts that current into voltage and amplifies it. The generated voltage, which is linearly proportional to the light, is measured by a data acquisition card (PCI-6036E, National Instruments Co., Austin, Texas, USA). If the particle is perfectly centered in the optical trap the laser beam diffraction pattern (Fig. 2.8), formed by the backscattered light, is on the center of the quadrant photodiode and the output signals values from all four quadrant are equal. If the trapped object is displaced from the center of the trap, the diffraction image on the QPD will also shift in a direction consistent with the particle's displacement, thus the light intensity on individual quadrant will not be equal to each other. By measuring the difference in the output signals of the QPD we can calculate the particles position within the trap with great precision.

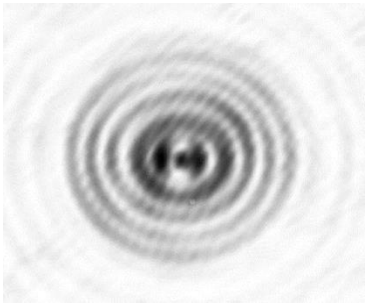

Figure 2.8. Diffraction image (750 × 600 pixels) of the backscattered light form a 1 μm particle in the center of the optical trap. The same image is projected on to the center of the Quadrant Photodiode.

The photodiode converts light in to current witch in turn has to be converted in to voltage by a transimpedance amplifier, in order to be measured by the acquisition hardware. Since these currents are very small, in the order of hundreds of nA, the gain the amplifier has to be in the order of 10^6 while at the same time it will have to have a bandwidth of at least 50 kHz and have low noise. Such an amplifier was not available commercially so it was constructed by the author (Fig. 2.9). All single photodiode quadrants are treated separately and have their own dedicated signal paths. The only exception is the reverse bias voltage applied to the common cathode (Fig. 2.10). Reverse bias reduces the capacitance of the photodiodes and therefore increases frequency bandwidth and reduces noise. The signal from a single photodiode anode is buffered by a FET transistor (Q1, BF862, NXP Semiconductors, Eindhoven, The Netherlands) in the source follower configuration (resistors R1 and R2), which provides high input impedance, which is essential in measuring low current signals.

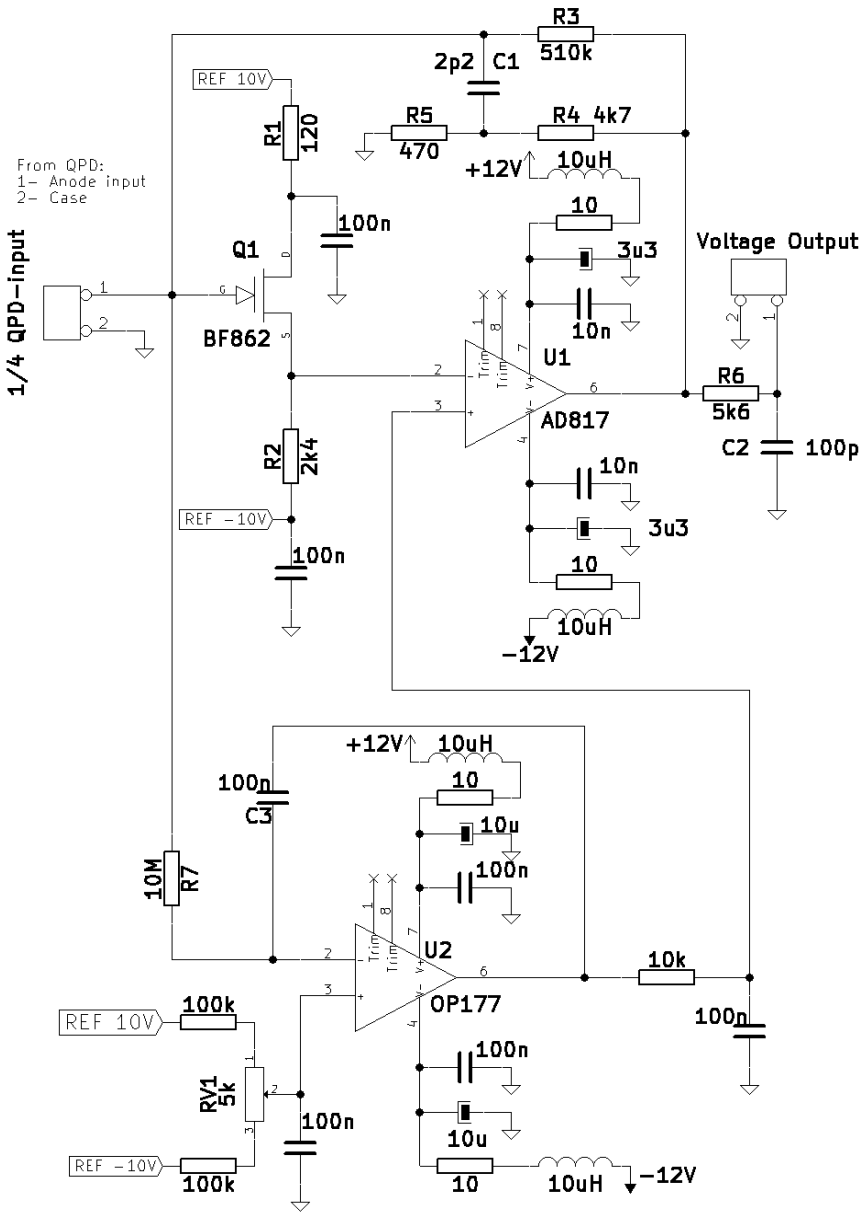

Figure 2.9. A diagram showing the optical signal detecting circuit for one single quadrant of QPD. The signal from the diode is converted by a transimpedance amplifier to calculate the relative position of the backscattered incident light beam in the QPD sensor. The whole optical signal detecting circuit consists of four photodiodes.

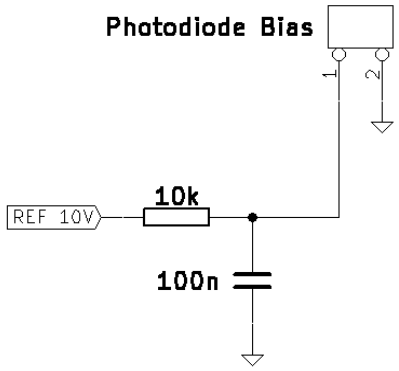

Figure 2.10. Schematic of the bias voltage supply tor the common cathode.

The high speed, low noise operational amplifier (U1, AD817, Analog Devices Inc., Norwood, Massachusetts, USA), in an inverting configuration, along with a negative feedback loop formed by resistor R3, amplifies and converts the photodiode current into voltage that is proportional to the light intensity. The capacitor C1 compensates for the photodiode capacitance and provides stability to the feedback loop. It is connected by the resistor divider formed by R4 and R5 that allow using higher value capacitors which is more practical. Direct current accuracy of the system is achieved by an additional low noise, high accuracy, operational amplifier (U2, OP177, Analog Devices Inc., Norwood, Massachusetts, USA), which drives the non-inverting input of U1, and therefore compensating its error. The offset voltage of the whole amplifier is adjusted to zero by means of the RV1 multi-turn potentiometer. The output signal of this amplifier additionally goes through a second order Butterworth filter and amplifier before being applied to the data acquisition card. The bandwidth of this circuit is set to 50 kHz to match the bandwidth of the acquisition card, and the overall transimpedance gain is 1MV/A.

The acquisition software computes two different output signals (S_X and S_Y) made by combining the voltages generated by the four photodiode amplifiers (V_1, V_2, V_3, V_4). The S_X and S_Y output signals are obtained from the following equations:

$$S_X = \frac{V_X}{P},$$
$$S_Y = \frac{V_Y}{P}, \tag{2.1}$$

where

$$V_X = (V_2 + V_4) - (V_1 + V_3),$$
$$V_Y = (V_1 + V_2) - (V_3 + V_4)\,, \qquad (2.2)$$
$$P = V_1 + V_2 + V_3 + V_4.$$

Signals S_X and S_Y are proportional to the X and Y position of the incident beam. If the particle is perfectly centred in the optical trap the laser beam is reflected on the center of the quadrant photodiode and the output signal values are zero. If the trapped object is displaced from the center of the trap, the backscattered light is not reflected in the middle of the quadrant photodiode and the signal values change. The light scattering of the sphere provides information about particle position when it is trapped in the focal point of the trapping laser beam.

The instrumental parameter control and data acquisition is performed by a dedicated program (Fig. 2.11) written by the authors in LabVIEW (LabVIEW Professional Development System 2013 Version 13.0f2 32bit, National Instruments Co.,

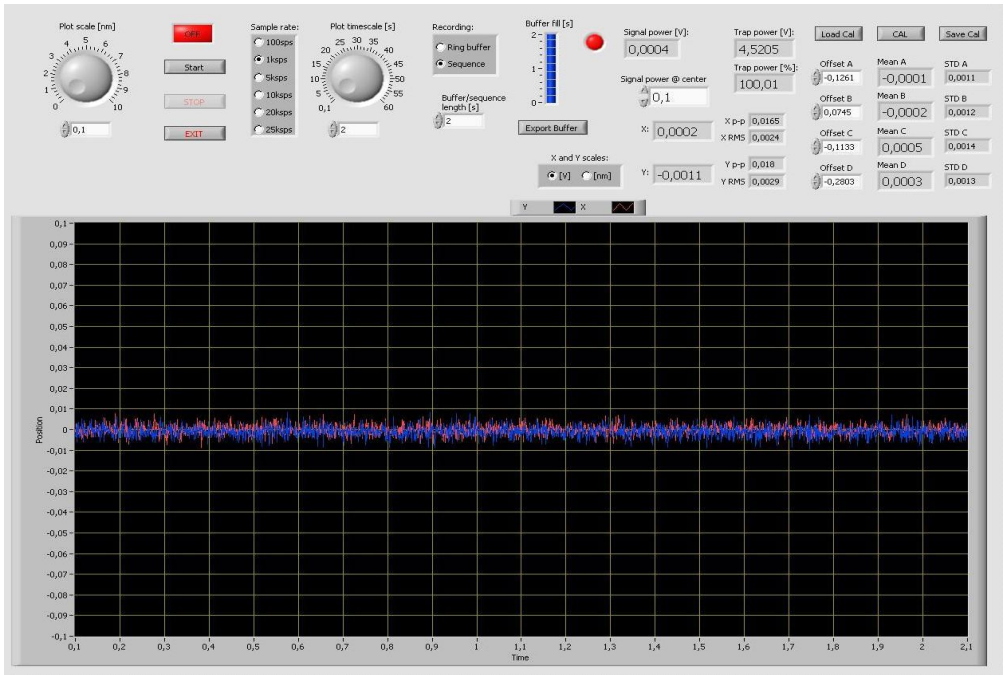

Figure 2.11. Screen capture of the acquisition software for the optical tweezers.

Austin, Texas, USA), Nova (Nova, NT-MDT, Limerick, Ireland) and the supplied camera software. The collected data are exported to Matlab (Matlab 8.3 R2015a, The MathWorks Inc., Natick, Massachusetts, USA) and Origin (Origin 9.0, OriginLab Corp., Northampton, Massachusetts, USA) software for further processing and statistical treatments.

2.2. Materials

All chemicals used were of analytical grade purchased from commercial suppliers. The experiments were performed using polystyrene particles with diameter of 1.0 μm dispersed in aqueous solution (Fluoro-Max Dyed Red Aqueous Fluorescent Particles, Thermo Scientific Inc., Fremont, California, USA). The microfluidic channels were fabricated out of polydimethylsiloxane (PDMS, Sylgard 184, Dow Corning Corp., Midland, Michigan, USA) by soft lithography. Surface-oxidized cover glass, obtained by exposing cover slips (24 × 24 mm, Carl Roth GmbH, Karlsruhe, Germany) to oxygen plasma (Zepto B, Diener Electronics GmbH, Ebhausen, Germany), was used to seal the PDMS channels. Acrylamide (AAm, Sigma Aldrich, Poznan, Poland), N,N'-methylene bisacrylamide (BIS-AAm, 99.5%, Sigma Aldrich, Poznan, Poland), ammonium persulfate (APS, 98%, Sigma Aldrich, Poznan, Poland), N,N,N',N'-tetramethylethylenediamine (TEMED, 99%, Sigma Aldrich, Poznan, Poland) were used without further purification to synthesize polyacrylamide hydrogel. All solutions were prepared using ultra-pure water with conductivity of 0.056 μS cm^{-1}. Water was deionized using a Hydrolab HLP purification system (HLP 5UV, Hydrolab, Wiślina, Poland).

3

Experiments and discussions

3.1. Laser alignment procedure

The capabilities of the Optical Trap and the detection system greatly depend on proper alignment of all the laser and their proper coupling to the objective. In order for the trap to be stable and as symmetrical as possible, the trapping laser axes has to be same as the axes of the objective. Moreover, due to the nature of the detection system, which relays on the backscattered light, the optical axes of the detection laser also has to be same with the one of the trapping laser. If not, the diffraction image will be distorted and the output signals of the photodiode highly nonlinear and thus it will be practically impossible to measure actual displacements of the trapped object. In order to have reliable results the available tolerances for positions of laser beams and lens axes in respect to each other are around 0.1 mm. This kind of required precision makes the traditional alignment methods "by eye" useful only at the first rough settings of the lasers, but for final alignment this method will not be sufficient. Thus, a special adjustment procedure was devised, which is based on a set of tubes with screens, a CMOS camera and a dedicated software for exact beam positioning. It is done after the first rough setting of the lasers are done when all the lasers are set so that they go through the aperture of the microscope objective. The configuration for final laser alignment is shown in Fig. 3.1.

In this configuration, the CMOS camera, now with an objective, and the White Light source are swapped, and the microscope objective is replaced with either a short or a long tube. Both Tube L1 and Tube L2 have threads that match the microscope's lens mount thread and fit exactly where the objective is. That way the optical axes of the optical trap goes through the center of the mounted tube. In order to visualize to position of the laser beam, both tubes have a mounted semi-transparent screen on their top side. The alignment procedure can be divided in to 4 main parts: 1. Finding the center of the Tube L1 and L2; 2. Alignment of the trapping laser; 3. Alignment of the detection laser; 4. Alignment of the fluorescent laser. Each part is described in detail below.

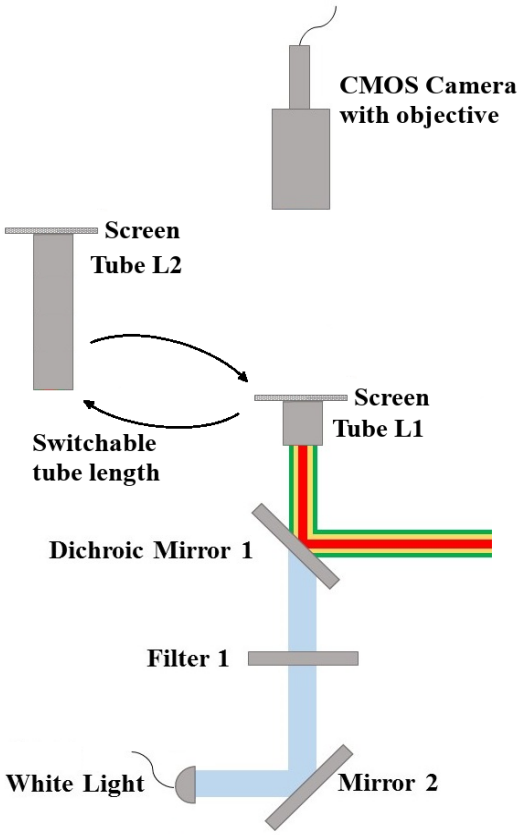

Figure 3.1. Diagram of laser alignment procedure. The tubs L1 and L2 with different length and a screen on top are exchanged in order to position the beam exactly in the optical axis of the microscope.

1. Finding the center of the tubes.
   In order to align the laser paths to the objectives optical axes, we first need to know where this axis is. To do that we first mount the Tube L1 and set the white light source to maximum output. This way it will illuminate equally the while aperture of the tube. The camera will record the image on the screen and the software will automatically find the center of the light spot on it. Next we change the Tube to L2 and analogically find the center of the light spot on its screen. The optical axes of the microscope will be the one that passes through the centers of both spots. This gives us the two positions to witch all the lasers have to be aligned.

2. Alignment of the trapping laser.
   The purpose of this part is to do the final alignment of the 1064 nm laser so that the Optical Trap can reach optimal parameters. The points to witch the laser has to be set are known form the previous part. The power attenuator is set so that the trapping laser will not over exposure the CMOS camera. First the Tube L1 is mounted and the center of the beam is recorded by the software. We then manipulate the Mirror M3 so that the beam will pass through the center of the tube. Next the Tube L2 is mounted and again the software records the beams position. Now by manipulating the Mirror M1 we adjust the beams position so that it will be in the center of the tube. After that we change the tube back to L1 and repeat the procedure until the beam is in the center of both tubes with 0.1 mm accuracy.

3. Alignment of the detection laser.
   The purpose of this part is to do the final alignment of the 633 nm laser so that the detection system can reach optimal parameters. The procedure is almost the same as in the previous section, the only difference is that now we manipulate Mirror M11 and M12 In order to position the detection laser in the center of the tubes.

4. Alignment of the fluorescence laser.
   The purpose of this part is to do the final alignment of the 532 nm laser so that the fluorescence illumination system can work in optical conditions. There settings are not so crucial to the operation of the optical tweezer and can be done just by observing the position of the laser spot on the sample.

The adjustment is done by Mirror M11 and M2. The size of the spot is determined by the Beam Expander 1.

When the alignment procedure has been finished the calibration procedure can begin.

3.2. Calibration

The calibration of optical tweezes is crucial in using this hybrid equipment as a quantitative sensor of forces. Despite the fact that the theory of operation of optical tweezers is well established, it is still very hard to accurately predict the actual forces acting on the trapped object. This is due to a couple of reasons. First of all it is hard to estimate the experimental conditions which are necessary to do the calculations.

The shape of the focal point, and therefore the light intensity gradient, will depend on the shape of the beam, position and angle at which it is entering the lens, the lens internal construction (which is a trade secret of the manufacturer) and all the losses along the optical path. Moreover, the distance between the lens and the channel wall, immersion oil, distance between the channel wall and the focal point, will all change the beam profile. All the mentioned parameters are necessary to make accurate calculations of the beam profile and yet are hard to estimate in practice. Another factor is the trapped objects size. The theories for objects which size is much smaller or much bigger than the wavelength of the trapping laser light are well described. But in most cases the trapped particles have diameters comparable with the wavelength and where is yet no good approach to this problem. Therefore, because of all the mentioned difficulties in calculations of the gradient force acting on the trap, it must be experimentally determined. There are several methods to calibrate an optical tweezers apparatus.

In this section we show the methods used and discuss the results of the calibration of QPD looking at the output signals – particle displacement relationship and the force calibration of the instrument.

The optical tweezers stiffness was evaluated over the widest possible range of trapping laser power level because we are aware of the importance of this technique to study also non-biological materials where the material damage due to the irradiation is negligible. Although the low cell damage induced by Nd:YAG 1064 nm laser [31] as well as the possibility to use high infrared laser power in biomolecules experiments [32] and the introduction of temperature controlled system have already been proven [33], a special attention was paid to explore the optical tweezers properties under 10 mW laser power level.

3.2.1. Detection system calibration

The first step to calibrate the trap was the analysis of quadrant photodiode response. In order to adjust the sample rate we analysed the noise of the quadrant photodiode at several frequencies when a motionless particle was in the focal point. A dispersion of polystyrene spheres 1.0 μm in diameter in polyacrylamide gel was used to place a fixed polystyrene sphere in the center of the trap and the 633 nm laser power was adjusted so that the total voltage of QPD was 4 Volts (V). The signals were recorded for 2 seconds at each single analyzed sample rate (Fig. 3.2).

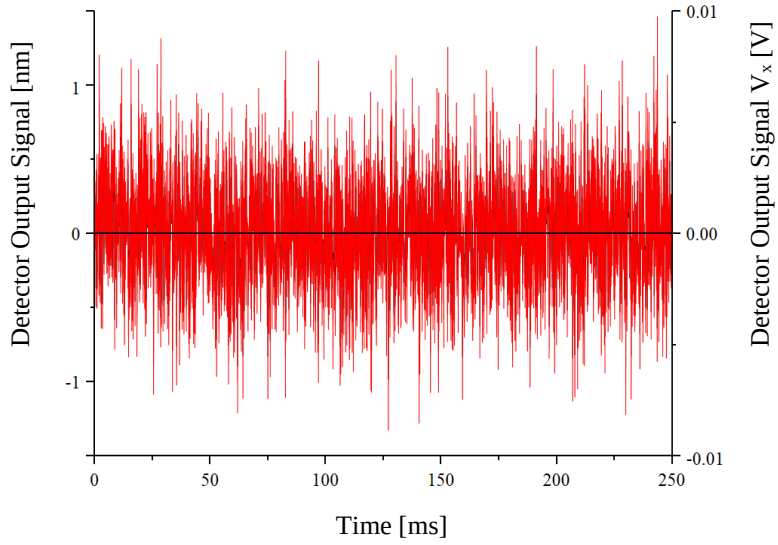

Figure 3.2. Diagram of photodiode output signal in *X* direction as a function of time when an immobilized 1.0 μm polystyrene bead is in the optical tweezers focal point. The curve shows the measured signal recorded at a rate of 5000 samples per second.

The recorded signals were analyzed expressing the instrumental noise as peak-to-peak value. The lower the acquisition rate, the less noisy the output signal is (Fig. 3.3). At high acquisition frequencies the analyses were affected by the noise. At low frequency the QPD was not able to detect fast and small particle displacement, therefore the selected sample rate of the detection system was set up at a maximum of 10.0 kHz in order to reach the optimum signal-to-noise ratio and speed. The peak-to-peak values obtained for S_x are comparable with those calculated for S_y. The output signals of the quadrant photodiode are clearly exposed to several sources of noise. Electronic noise, mechanical, acoustic vibrations and laser instabilities can be minimized by applying some experimental precautions but it cannot be removed completely. However, much higher amplitude of noise is generated by the Brownian motion of trapped object.

In order to calibrate the optical tweezers using the backscattered light collecting sensor as particle position sensor we need to fully know the response of QPD as a function of bead displacement. A 1.0 μm diameter polystyrene particle stuck in polyacrylamide gel was used to study the sensitivity of the quadrant photodiode. The bead was placed in the center of the trap. The piezo stage, on which the sample was

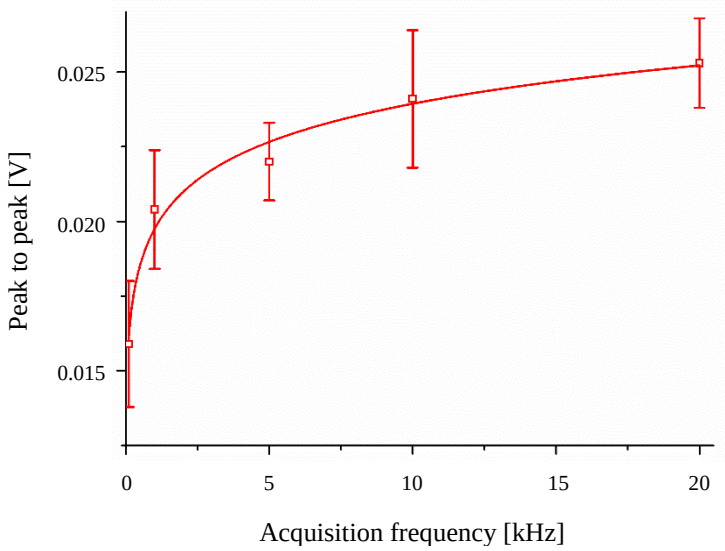

Figure 3.3. Measured peak to peak value of S_X noise for different acquisition frequencies. Each data points is an average of 40 measurements in which the S_X signal was recorded for 2 seconds. Error bars represent the standard deviation (from Ref. [1].).

mounted, allowed us to move the polystyrene sphere with a stepwise motion. We recorded the values of S_x and S_y after each particle displacement generated by a small and quick piezo stage movement when the bead passed through the tweezers. The particle displacements were generated by a sequence of back and forth stage movements and the measurements were carried out starting from –100 nm to +100 nm. Each measurement point was repeated 100 times. The central parts, of the typical *S*-shape detector response curves, are reported in Fig. 3.4.

There are several factors that can affect QPD sensitivity, one of the most important is the profile of the beam. The backscattered light pattern changes with the relative position of the incident detection laser beam on the trapped particle. The impact of this typical scattered light behavior is evident in the output signals/particle displacements graph: the response is linear for displacements in the range of ±100 nm. Therefore, only the central zone of the graph was used to calibrate the quadrant photodiode sensitivity and trap stiffness, by calculating the slope of the best linear fit. The slope of the fit lines (α_X, α_Y) for S_X and S_Y are respectively 0.0026 and 0.0031 in arbitrary units.

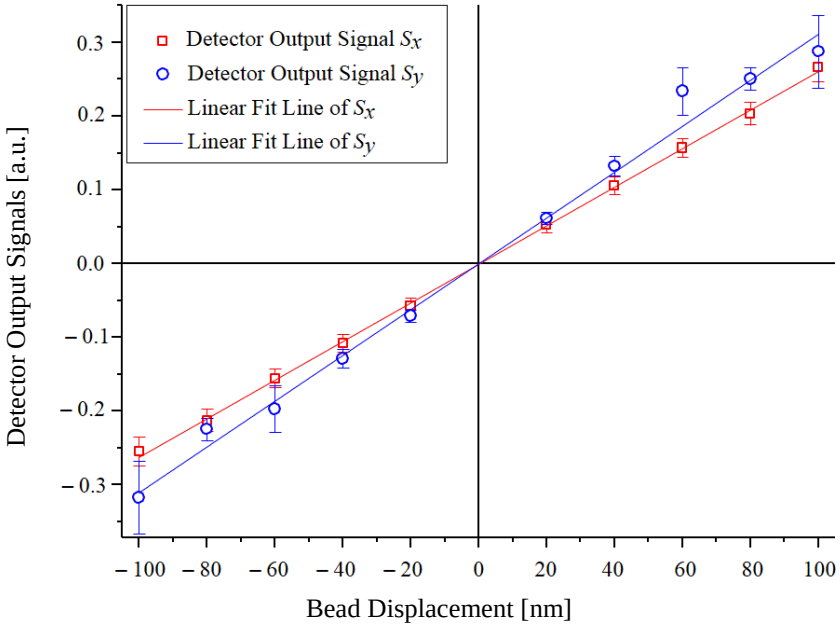

Figure 3.4. Quadrant photodiode output signals (S_x and S_y) versus particle displacement curves recorded by moving the bead through the optical trap. The displacement is relative to the centre position of the trapped bead. The output signals are zero when the object is in the trap centre. The curves were obtained using 1.0 μm polystyrene particles in water.

The particle displacements (X, Y) in nanometers can be calculated with the following equations:

$$X = \frac{S_X}{\alpha_X}, \qquad Y = \frac{S_Y}{\alpha_Y}. \tag{3.1}$$

The presence of backscattered light pattern asymmetry is responsible for the difference in sensitivity between X and Y direction as well as the non-linear response for bead displacements higher than 100 nm from the centre of the trap. The sensitivity of the quadrant photodiode is also affected by the ratio of light spot radius and QPD radius to the distance between the centre of the detector and the reflected beam.

3.2.2. External Force Calibration

The external force calibration method quantifies the amount of force applied by the trapping laser on the bead using a specific instrumental and environmental configuration. The analysis of the relationship between the particle position and the quantity of an applied external force on the trapped sphere under controlled conditionis one of the most effective strategies to calibrate the trap. The trapped particle-optical tweezers system can be considered as a Hookean spring where the force acted on the sphere is proportional to the particle displacement from the central trap position and to the trap stiffness as described in Eq. (1.6). According to this model, it is possible to calculate the trap stiffness by observing the particle displacement while applying on it a known external force. Usually the sphere displacement is proportional to the amount of force trying to perturb the system equilibrium. Hydrodynamic drag, resulting from an applied flow of water around the trapped particle, acted as the external force. The experiments were performed inside a tailored PDMS microfluidic (Fig. 3.5) chip filled with water solutions at temperature 295 K. In order to eliminate possible influences of any stray flow in the channel, all the measurements where preformed in special round wells with only one entrance. When the particle was captured by the OT, it was dragged in to one of the wells where the measurement took place. The particle was trapped 5 μm far from the glass wall and at least 50 μm away from any surface in order to avoid the wall effects and to ignore Faxen's correction [26].

The experiment was performed at the system equilibrium in order to avoid any unexpected convective flow. The flow Reynolds number based on the particle diameter was below 10^{-3}. In the low Reynolds number regime the external drag force (F_{ext}) acting on a bead can be easily quantified using Stokes' law:

$$F_{\text{ext}} = 6\pi\eta v R, \tag{3.2}$$

where η is the dynamic viscosity of the water, v is the fluid velocity and R is the trapped sphere radius.

The flow of the fluid around the trapped sphere was applied by moving the piezo stage on which the channel was mounted. The external force was quantified using the method proposed by Mills et al. [34] when the AFM piezo stage was moved at different constant velocities translating the chamber by steps of 100 μm in the X and Y direction. The system was analyzed at several values of external force maintaining the step displacement constant and changing the stage velocity; at least 100 events were

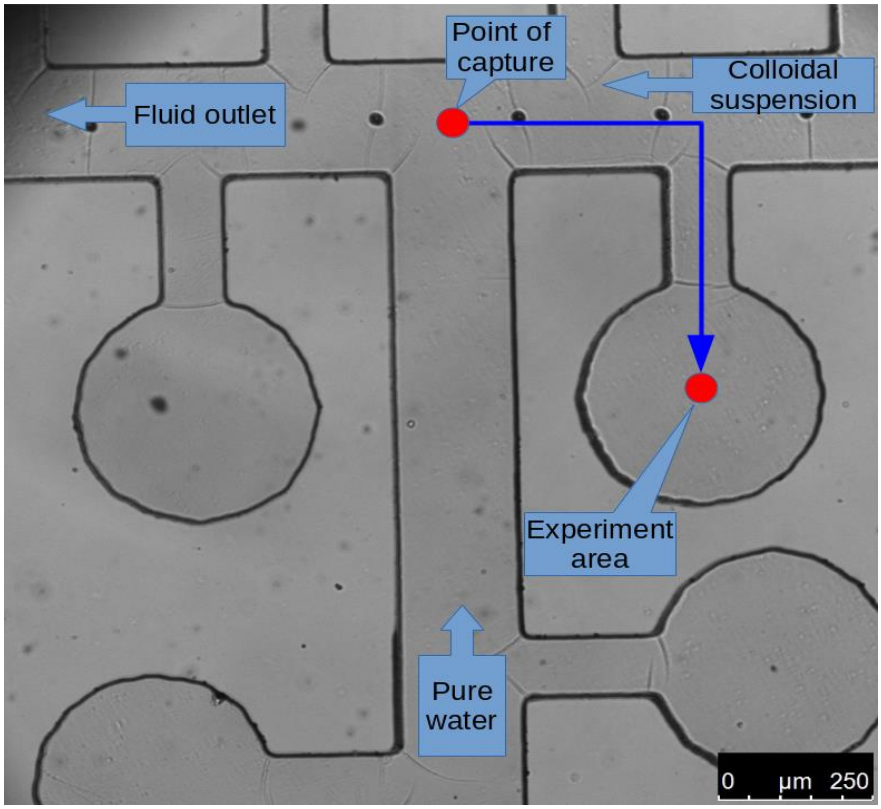

Figure 3.5. Picture of a microfluidic channel used in the experiments. The large channels form a T junction, through one of the arms flows pure water, and through the second a solution of particles. The round wells with only one entrance provide a flow-free chamber where the measurements take place once a trapped particle is dragged into them by the optical tweezer. Multiple wells allow conducting more than one experiment in the same microchannel.

taken into account in the stiffness calculation in each analyzed experimental condition. The optical tweezers stiffness was calculated at 15 different trapping laser power levels by analyzing the recorded output signals of the QPD particle position detector (Fig. 3.6). The results shown in Table 3.1 were averaged over few experiments repeated using the same experimental parameters.

The trap stiffness (Fig. 3.6) increases linearly with the trapping laser intensity. The optical tweezers calibrations show the stiffness asymmetry caused by the polarization of the laser beam. These results are in agreement with theoretical and previous experimental results achieved by Rohrbach [35], where the relationship between the

asymmetry coefficient and several experimental parameters (e.g. power and wavelength of laser and particle dimension) was proven.

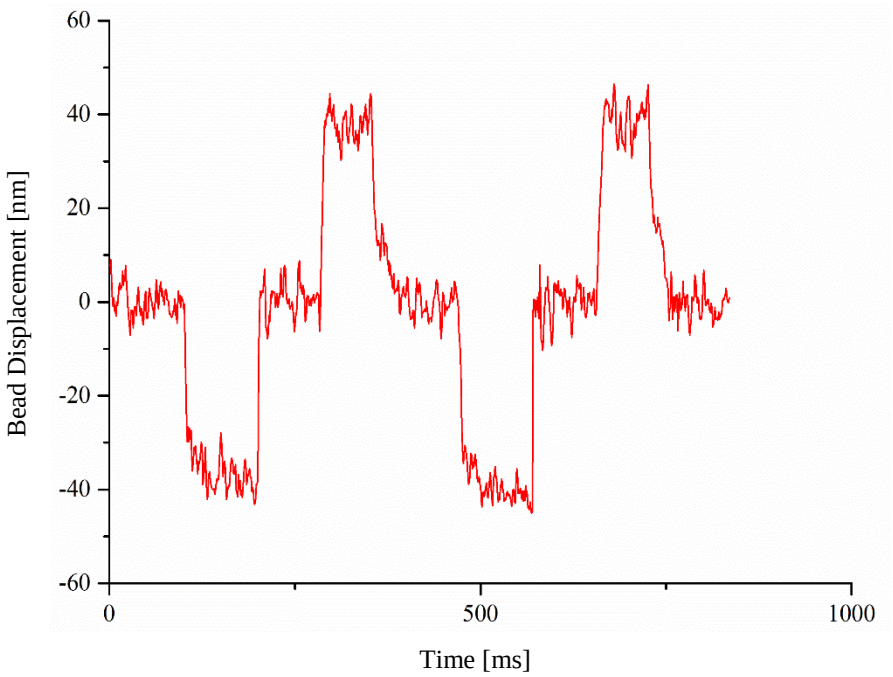

Figure 3.6. Bead position along the *X* axis vs time during the external force calibration. A 1.0 μm diameter polystyrene bead is trapped using the infrared laser (40 mW) and the sample is moved transversally back and forth at constant velocities (1300 μm/s). The piezo stage is set up to make one 100 μm movement each way with a 100 ms delay between every single stage translation.

Table 3.1. Traversal escape force measured from 1.74 mW to 4.24 mW of trapping laser power.

Trapping laser power [%]	Axes direction	Escape force [pN]	Escape force standard deviation [pN]
1.74	*X*	5.27	0.40
2.62	*X*	7.70	0.23
4.24	*X*	11.87	1.13
1.74	*Y*	5.26	0.14
2.62	*Y*	7.74	0.03
4.24	*Y*	9.63	0.19

When the piezo stage movement was increased above a certain threshold, the external force overcame the trapping laser force and the bead escaped from the optical tweezers. The escape force is defined as the highest force applicable to the trapped objects therefore it defines the upper force limits of optical tweezers. The higher the trapping laser power, the higher the escape force (Table 3.1). We found that our optical tweezers system has a maximum escape force of 11.87 pN using a 4.24 mW trapping laser.

3.2.3. Equipartition Calibration

As we mentioned before, the trapped particle behavior can be described as a mass on a spring system where the spring constant is the trap stiffness. Therefore, the system can be considered as a sphere in a harmonic potential. The trapped bead oscillates randomly near the focal point of the laser beam when it is in thermal equilibrium. The particle fluctuations are due to the Brownian motion which tends to displace the bead stochastically. The bead spatial position is well-described by a Gaussian function centered in the focal laser point where the width of the Gaussian curve is associated with the trap stiffness, and the probability to find the particle near the center is higher in stiffer optical tweezers systems. The particle is stable when the force applied by the laser to the trapped object overcomes the forces generate by collisions of the environmental molecules to the beads, confining the Brownian motion in the trap region. The Brownian motion of a particle is directly proportional to temperature. Consequently, it is possible to estimate the trap stiffness by tracking the particle position and calculating the displacements from the average position point in a well-known thermal condition. The equipartition theorem defines the average translational kinetic energy of a particle for each translational degree of freedom as ½ *kBT* where *kB* is the Boltzmann constant and *T* is the absolute temperature. According to this theorem it is possible to evaluate the trap stiffness (*K*) by solving the equation:

$$K_x = k_B T / \langle \Delta x^2 \rangle, \qquad K_y = k_B T / \langle \Delta y^2 \rangle, \tag{3.3}$$

where $\langle \Delta x^2 \rangle$ and $\langle \Delta y^2 \rangle$ are statistical variances in the particle position.

The displacements of a 1.0 μm polystyrene particle in water were recorded for 20 seconds with a fixed acquisition frequency (10 kHz) at several trapping laser power levels. The trap stiffness was calculated averaging 30 series of data acquisitions for

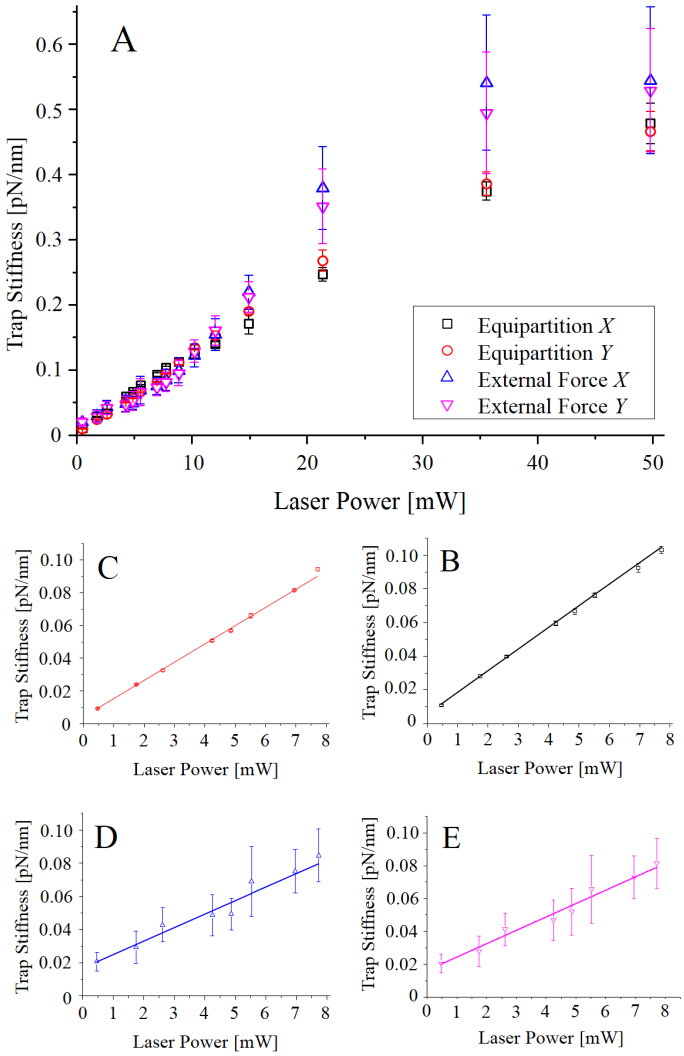

Figure 3.7. Graphs showing the stiffness of the trap in *X* and *Y* direction, as a function of the trapping laser power, for a 1.0 μm polystyrene bead. Graph (A) show data obtained by equipartition and external force measurement method for both *X* and *Y* axes for trapping laser power in the range from 0.5 mW to 50 mW. Next graphs show the trap stiffness for the laser power in the range from 0.5 mW to 8.00 mW using equipartition method in the *X* axis (B) and *Y* axis (C) and using external force in *X* axis (D) and *Y* axis (E). Each point in the graph is the average of 30 measurements (from Ref. [1].

each laser power settings (Fig. 3.7). The temperature of the fluid was evaluated using a pre-calibrated thermocouple sensor located few micrometres far from the analyzed bead and assuming that the temperature in this point was similar to the trap temperature [36]. In this experiment the power of 1064 nm laser was set starting from 0.50 mW and then was gradually increased to 50.0 mW of the total trapping laser power. We noticed that due to the temperature rising at high laser power level, the difference between the focal point where the particle is confined and the surrounding liquid created large convective instabilities in the system, forcing us to extend equilibration time. The temperature estimation has a crucial role in the equipartition calibration. The stiffness standard deviation rose in proportion to the laser power.

The results obtained for laser power below 10 mW using the equipartition method confirm the previous calibration data highlighting the strong dependence between the laser power and the optical tweezer's stiffness. The reason why the trap's stiffness does not decay to zero when the trapping laser power is equal to zero is the influence of the detection laser, which forms a trap of its own and despite its low power, at these force scales it can't be neglected.

3.3. Optical tweezers atomic force microscopy double probing

One of the most interesting applications is to use tweezers in order to manipulate single objects (e.g. nanomaterials and cells). The main achievement of the optical trapping nanomanipulation was to develop a selective cell sorting process with the aim to purify samples and to study the biological behavior of single selected cells. Nanomanipulation can also be useful to organize, assemble and locate complex hierarchical structures composed through optical tweezers manipulation. The proposed study is based on the capabilities of sorting single nano-objects using optical tweezers. In order to demonstrate the capabilities of the AFM/OT system we prepared a particle nanostructure using the dragging force of the trapping laser and we simultaneously scanned the sample using AFM.

First of all, the glass slide used in this experiment was silanized with method proposed by Labit et al. [37]. The chemically functionalized glass coverslip was used in this experiment in order to increase the interface interaction between the 1.0 μm polystyrene bead and the substrate. During this experiment, the trapping laser power was set to 10 mW in order to reach a high trapping efficiency and avoiding convective flow or other undesirable phenomena which can affect the nanomanipulation. First,

five polystyrene particles were maneuvered and isolated from the colloidal system, than the selected particles were individually confined in a clean well and dragged to the glassy bottom in order to form a straight line of particles. The force exerted by the trapping laser is strong enough to push the particle to the glass wall and the adhesion effects allow immobilizing the particle on the substrate. The glass surface modification plays a crucial role in the proposed experiments. The attractive force between the positive charged surface and the negative charged polystyrene has an extremely beneficial influence on the stability of the produced structure. The AFM/OT system was used to collect AFM topographies of the area selected for conducting the experiment before and after the particle deposition as well as the surface of the single dragged particles.

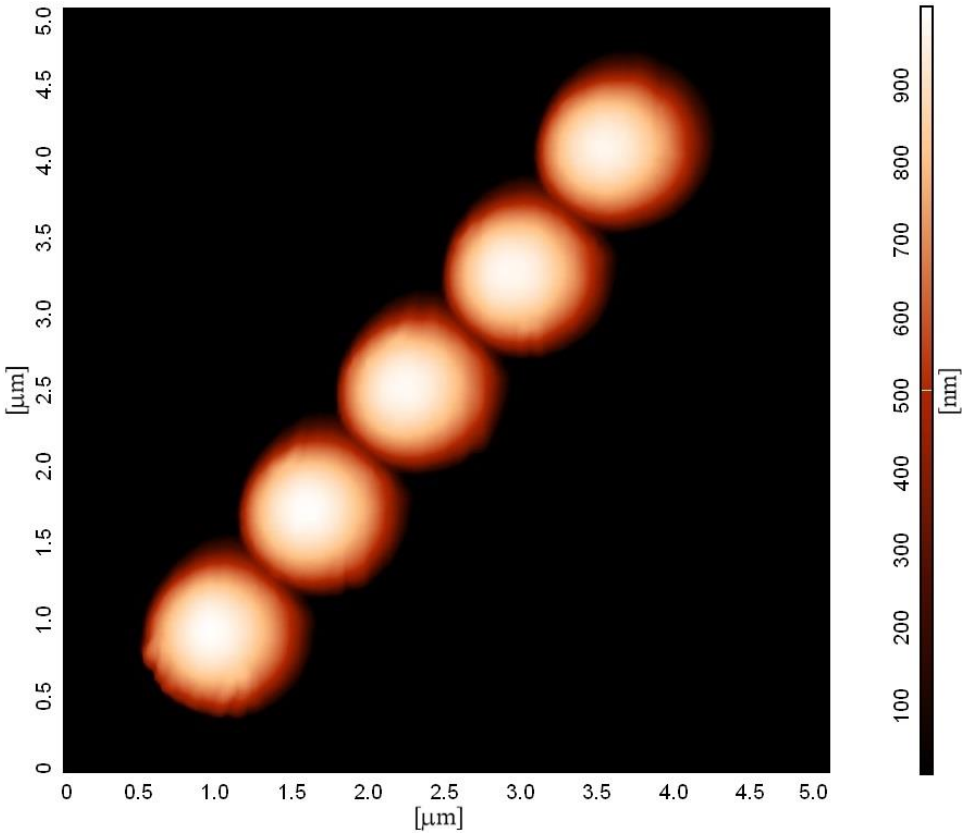

Figure 3.8. Topography image of polystyrene particles immobilized onto a special functionalized glass substrate obtained in a semicontact mode AFM using HA-NC cantilever (from Ref. [1]. © IOP Publishing. Reproduced with permission. All rights reserved).

Topography images of immobilized particles were acquired in water using the tapping mode of AFM at a scan frequency of 0.25 Hz. We have tried to minimize the force applied by the AFM probe on the sample by using a cantilever with a spring constant of 2.5 N/m (HA_NC cantilever, NT-MDT, Limerick, Ireland). Figure 3.8 shows a 5 × 5 μm AFM image of the ordered layer of polystyrene particles developed using the dragging force of the optical tweezer system.

This experiment allows studying the surface properties of the particles and substrates taking into consideration one single particle-surface interaction and studying single events to characterize locally the studied materials.

3.4. Atomic force microscopy and optical tweezers double probe force sensor

The knowledge of interactions of colloidal particles with their surrounding medium and with each other is crucial to understand their behavior in crowded environments such as cells and other biological materials. The equilibrium state and the hydrodynamic properties of colloid systems in an aqueous medium are affected by several environmental parameters (e.g. the addition of salt influences the stability of colloids). An explanation for this fact was given by the Derjaguin-Landau-Verwey-Overbeek (DLVO) theory studying the surface charges at interfaces and the factors that affect the electrostatic double-layer force [38]. As such the effects of ion concentrations and their type can't be neglected. For particles with dimensions in the range of nanometers the effects of ionic double layer, steric effects and kinematic slip on the fluid-wall boundary condition greatly influence their mobility. Most experiments that characterize these kinds of suspensions measure only the global parameters, used only to evaluate the effective mobility coefficients. In this experiment we demonstrate the ability of optical tweezers enabling nonintrusive measurements of forces, in the range of femtonewtons, acting on suspended in liquid polystyrene particles. Its coupling with AFM allows for accurate measurements of the surface and geometry as it was demonstrated in the previous chapter. In the following experiment the possibility to use the hybrid AFM/OT instrument to quantify force in the femtonewton scale is demonstrated. This kind of research is very popular right now and this instrument will be helpful to elucidate the details of the phenomena that regulate the colloids stability as well as the properties of molecules attached to their surface.

The colloidal probe cantilever used in this experiment was built by the use of the "Cantilever-moving technique" developed by Gan [39] in which a single fluorescent

5.5 μm particle was glued to the end of a tip-less AFM cantilever using a small amount of epoxy glue and the AFM head acted as a micromanipulator (Fig. 3.9).

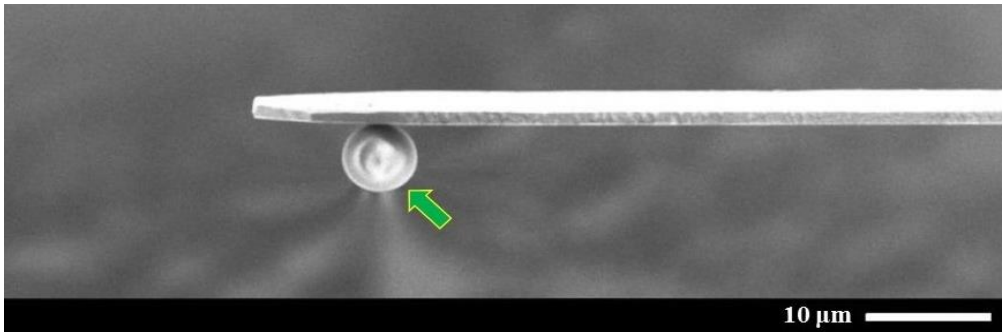

Figure 3.9. SEM micrograph of the 5.5 polystyrene particle mounted on the tipless AFM cantilever.

The experiments were performed inside a tailored PDMS microfluidic (Fig. 3.10) chip filled with water solutions at temperature 295 K. In order to eliminate possible influences of any stray flow in the channel, all the measurements where preformed in

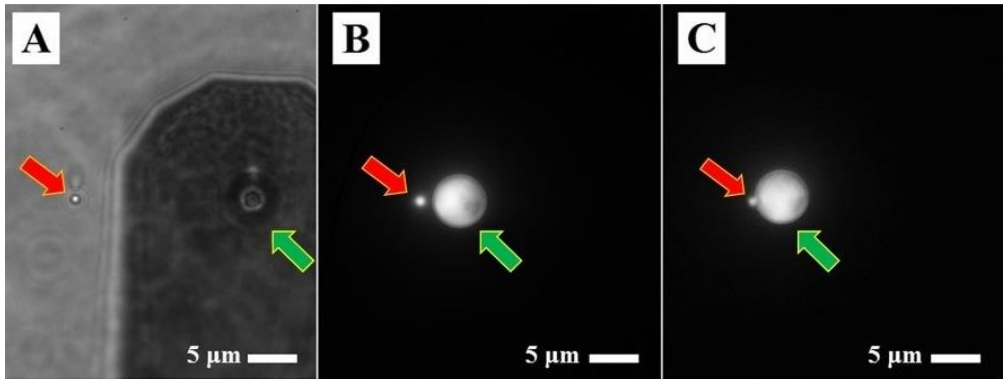

Figure 3.10. Example picture of produces AFM colloidal probes and images taken during tone of the experiments. A – 1.0 μm polystyrene particle trapped in the OT a few micrometers from the cantilever. B – Translation of the probe in the direction of the trapped particle. C – The particle glued to the cantilever approached the surface of the trapped particle. Picture A was collected using a white light while pictures B and C were recorded using fluorescent particles excited by the green 532 nm wavelength laser. The red arrows indicate the position of the optically trapped 1 μm particle and green arrows the 5.5 μm particle attached to the AFM cantilever.

special round wells with only one entrance. When the particle was captured by the OT, it was dragged in to one of the wells where the measurement took place. The single fluorescent colloid sphere fixed at the end of the tipless cantilever and a 1.0 μm fluorescent polystyrene sphere confined in the optical trap using 6.5 mW laser power (Fig. 3.10 A – B – C).

The experiments were carried out by approaching the trapped particle with the AFM particle probe at a constant velocity of 200 nm/s in pure water and recording the displacement of the particle in the optical tweezers. This displacement was later calculated in to force, and the results are shown in Fig. 3.11.

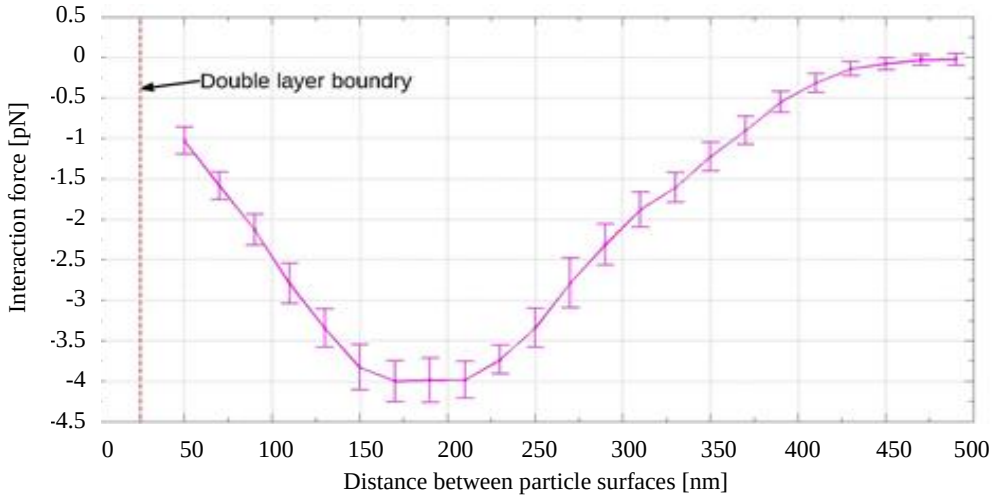

Figure 3.11. Interaction forces between two particles in pure water, as a function of the distance between their surfaces.

The same experiment was repeated in 0.01 mM and 1 mM solution of KCl in water. The particle approaches were performed after 30 minutes from the liquid introduction into the channel to reach the thermal equilibrium that was monitored by using a thermocouple inserted into the microchip channel. More than 30 approaches were performed per each analyzed environmental condition in order to have statistically significant results. The results of the experiments with KCl are shown in Fig. 3.12.

The size and shape of the polystyrene particle mounted on the tipless cantilever has been measured by the use of SEM before the experiment. The position of the particles and their separation distance have been evaluated by analyzing the white

light and fluorescence images obtained by the CMOS camera, using a custom-made Matlab program for finding center of the particles.

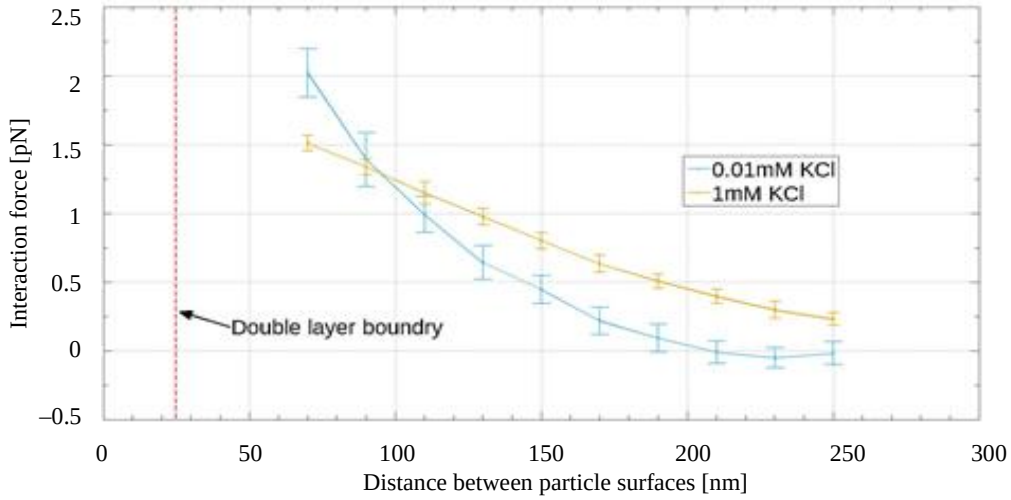

Figure 3.12. Interaction forces between two particles in two different concentrations of KCl in water, as a function of the distance between their surfaces.

The measured force–distance relationships between two particles in different aqueous solutions of KCl (Figs. 3.11 and 3.12) proves that the instrument is capable of qualitatively measuring forces with a subpiconewton resolution with good reproducibility. The developed combined atomic force microscopy and optical tweezers has higher resolution and reproducibility compared to a standalone AFM in the analysis of particle interaction forces [40]. The obtained data confirms that the behavior of colloidal systems observed experimentally agrees with the theoretical predictions. The DLVO theory assumed that the interaction between two particles is due to the sum of the electrostatic double-layer repulsion and the van der Waals attraction. In pure water, long range attraction is clearly measured. At low salt concentration the double-layer repulsions are stronger than in pure water and the single polystyrene particles are stable. The particle stability increases with the KCl concentration in the micromolar range. In the experimental results, in all the studied systems, no interaction forces between the polystyrene particles could be observed at distances exceeding 450 nm.

4

Conclusions and outlook

Atomic force microscopy is a versatile technique capable of covering a broad range of applications, but it is not able to detect small forces on the femtonewton scale due to technical limitations and restrictions. Based on this consideration, we have designed and developed a type of AFM-optical tweezers apparatus in order to build a high resolution imaging instrument capable to confine micro- and nanomaterial and to lower the force limit of detection of AFM. The successful development of the equipment has been described in detail and the calibration of the instrument has been presented in this study.

We have shown how important the optics and electronic arrangement and settings are to achieve the high temporal and spatial resolution required during the force measurements. In this article we proposed an improvement of the trapped particle position detection system. We also showed an integrated system based on the collection of backscattered light by a quadrant photodiode. A comprehensive explanation of the sensor has been provided and the high sensitivity and resolution of the detector has been confirmed by the experimental calibration. Nevertheless, it is possible to further increase the sensitivity and the resolution by improving the acquisition data system.

The optical tweezer stiffness usually depends on several experimental parameters such as the shape, refractive index and position of the trapped object, profile and intensity of the trapping laser and the sample medium refractive index. That is the reason why the optical tweezers stiffness was calculated by two different methods in the same experimental condition and the relationship between trapping laser power and applied force was investigated. The basic calibration presented in this paper was the external force method. The results demonstrate that the minimum applicable and detectable force of the proposed optical tweezers is at least one order of magnitude better than the best result achieved by AFM. The external force method has allowed us to measure the highest applicable and detectable force by calculating the force necessary to escape the trapped particle from the optical tweezers focus spot. The escape force is proportional to the trapping laser beam power (Table 3.1) and this confirms the possibility to analyze forces up to 11.87 pN using a 4.24 mW laser power and to use optical tweezers in a force range below the limit of detection of AFM. An alternative

calibration method based on equipartition was carried out and the results obtained confirm the high sensitivity and resolution of the instrument. The equipartition method is easy enough to implement, it is very fast and does not require any additional equipment. After proper calibration it can be used to evaluate local temperature or/and to extend evaluation of Brownian motion into inertial (ballistic) regime.

We found that the calibration methods using external force and equipartition performed equally well in the reported experimental conditions. The reproducibility of calibration methods is expressed as the standard deviation of trap stiffness. The standard deviations obtained using external force are greater than the values calculated by the equipartition method for lower laser power (0.5 mW and 8.0 mW). It evidences the advantage of the method based on of the trapped particles Brownian motion study when the trap weakness disturbs accuracy of the external force calibration technique. Indeed, when the laser is set on a lower power than 0.5 mW the force applied by the laser beam was frequently overcome by the drag force resulting from the slowest possible applied stage movement. Moreover, when the laser power is lower than 3 mW the fluctuation around the center of the trap is comparable with the displacement of the particle due to the external drag force, affecting the precision of the result reached by using the external force method. Our study pointed out that the trap stiffness values obtained using equipartition calibration have a directly proportional relationship with the trapping laser power and that the results are very precise and accurate in the region in which the force of the trap is weak. The curves obtained between 0.5 mW and 8.0 mW are well fitted by a line and the relative standard deviations rarely exceed 3% of the calculated trap stiffness. On the other hand this method appears to be less useful to measure the properties of the trap when trapping laser is set up at higher trapping power than 20 mW and this is quite evident considering that the stiffness-laser power correlation became non-linear at this point. We can therefore say that the use of few calibration techniques is crucial for measuring the optical tweezer's stiffness in a wide range of applied trap power.

The trapping efficiency of the optical tweezers is very good and it is capable of manipulating non spherical objects like nanofibers even at very low differences in refractive indexes of the material and the medium (Fig. 4.1).

External force and equipartition calibration methods provide us only with information regarding the stiffness of the trap in the plane perpendicular to the incident laser's direction. Therefore, a further three dimensional calibration has to be performed in order to fully understand the forces involved in particle confinement. In

future we would like to measure the trap stiffness using particles of different composition and size.

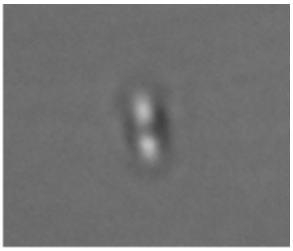

Figure 4.1. A short fiber trapped by the optical tweezers. The refractive index of the medium is 1.43, and the object index of refraction is 1.52.

The presented setup allows manipulating biological systems of greater complexity and to analyze their material properties and behavior from a different point of view, for example trapping and manipulating intracellular objects and probing the cell surface by AFM cantilever, simultaneously (Fig. 4.2).

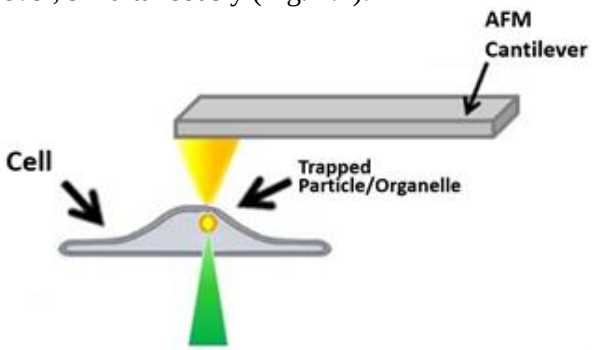

Figure 4.2. Schematic of a proposed double probe technique to study cell biology with AFM and OT at the same time.

Such measurements can be vital in the study of the microbiological and bimolecular aspects of many diseases such as cancer and Alzheimer. Previous AFM nanoindentation studies prove that the variation of Young's modulus values along the same fibril is low, suggesting a similar supramolecular structure along the fibril [41].

This double probe instrument will be useful for studying the mechanical properties of single long chain molecules, fibers and rods as it allows analyzing the effect of the twisting and/or stretching (Figs. 4.3 and 4.4). By attaching a molecule (or a one-dimensional nanomaterial) to the AFM cantilever on one side and to a paramagnetic

bead on the other it is possible to twist it using a rotating magnetic field to torque the bead. In this experiment the optical tweezers will act as a manipulator and the atomic force microscope as a force and spatial sensor (Fig. 4.3).

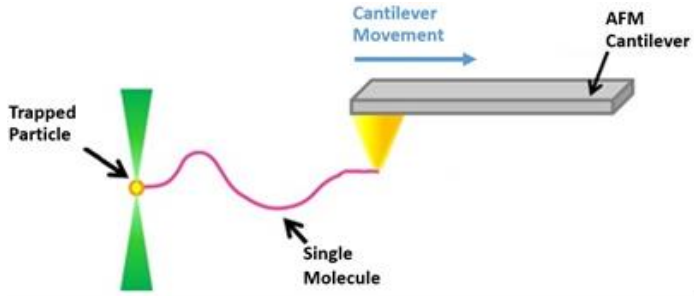

Figure 4.3. Schematic of a proposed technique to study mechanical properties of single molecules and polymers by stretching.

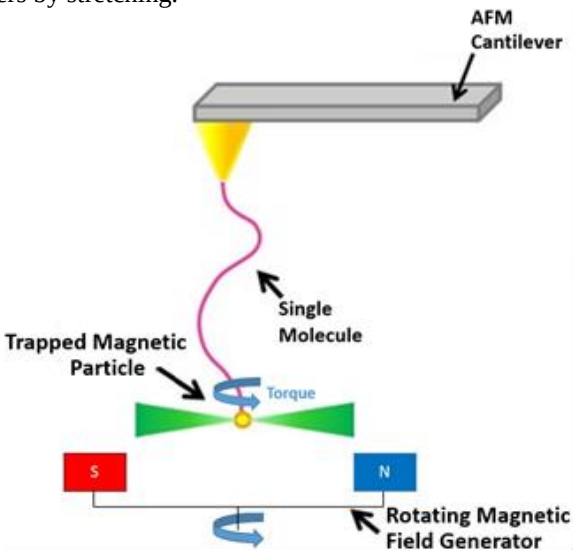

Figure 4.4. Schematic of a proposed technique to study mechanical properties of single molecules and polymer by twisting.

The combination of atomic force microscopy and optical tweezers in one single piece of equipment has already given us the ability to obtain images, to manipulate and quantify the motion and the forces directly in the same sample. In conclusion we have presented and tested an innovative instrument that, to the best of our knowledge, is currently the first combined atomic force microscope-optical tweezers.

Bibliography

1. F. Pierini, K. Zembrzycki, P. Nakielski, S. Pawłowska, and T. A. Kowalewski. Atomic force microscopy combined with optical tweezers (AFM/OT). *Meas. Sci. Technol.*, 27:025904-1-11, 2016.
2. A. Janshoff, M. Neitzert, Y. Oberdorfer, and H. Fuchs. Force spectroscopy of molecular systems – Single molecule spectroscopy of polymers and biomolecules. *Angew Chem. Int. Ed.*, 39(18):3212–3237, 2000.
3. G. Binnig, C. F. Quate, and C. Gerber. Atomic force microscope. *Phys. Rev. Lett.*, 56(9):930–934, 1986.
4. S. Sevim, S. Tolunay, and H. Torun. 2014 Micromachined sample stages to reduce thermal drift in atomic force microscopy. *Microsyst. Technol.*, 21(7):1559–1566, 2015.
5. A. Beyder, C. Spagnoli, and F. Sachs. Reducing probe dependent drift in atomic force microscope with symmetrically supported torsion levers. *Rev. Sci. Instrum.*, 77:056105-1-3, 2006.
6. N. K. Voulgarakis, A. Redondo, A. R. Bishop, and K. Ø. Rasmussen. Sequencing DNA by dynamic force spectroscopy: limitations and prospects. *Nano Lett.*, 6(7):1483–1486, 2006.
7. K. C. Neuman and A. Nagy. Single-molecule force spectroscopy: optical tweezers, magnetic tweezers and atomic force microscopy. *Nat. Methods*, 5(6):491–505, 2008.
8. A. Ashkin. Acceleration and trapping of particles by radiation pressure. *Phys. Rev. Lett.*, 24(4):156–159, 1970.
9. A. Ashkin, J. M. Dziedzic, J. E. Bjorkholm, and S. Chu. Observation of a single-beam gradient force optical trap for dielectric particles. *Opt. Lett.*, 11(5):288–290, 1986.
10. W. Nasalski. Optical beams at dielectric interfaces – fundamentals. *Institute of Fundamental Technological Research*, ISBN 978-83-89687-26-5, 2007.
11. K. C. Neuman and S. M. Block. Optical trapping. *Rev. Sci. Instrum.*, 75(9):2787–2809, 2004.
12. A. Ashkin. Forces of a single-beam gradient laser trap on a dielectric sphere in the ray optics regime. *Biophys. J.*, 61(2):569–582, 1992.
13. N. Malagnino, G. Pesce, A. Sasso, and E. Arimondo. Measurements of trapping efficiency and stiffness in optical tweezers. *Opt. Commun.*, 214(1–6):15–24, 2002.

14. D. G. Grier. Optical tweezers in colloid and interface science. *Curr. Opin. Colloid Interface Sci.*, 2(3):264–270, 1997.
15. J.-C. Meiners and S. R. Quake. Femtonewton force spectroscopy of single extended DNA molecules. *Phys. Rev. Lett.*, 84(21):5014–5017, 2000.
16. J. Berthelot, S. S. Acimovic, M. L. Juan, M. P. Kreuzer, J. Renger, and R. Quidant. Three-dimensional manipulation with scanning near-field optical nanotweezers. *Nature Nanotech.*, 9:295–299, 2014.
17. K. Visscher, M. J. Schnitzer, and S. M. Block. Single kinesin molecules studied with a molecular force clamp. *Nature*, 400:184–189, 1999.
18. M. J. Comstock, T. Ha, and Y. R. Chemla. Ultrahigh-resolution optical trap with single-fluorophore sensitivity. *Nat. Methods*, 8(4):335–340, 2011.
19. J. Lipfert, G. M. Skinner, J. M. Keegstra, T. Hensgens, T. Jager, D. Dulin, M. Köber, Z. Yu, S. P. Donkers, F.-C. Chouc, R. Das, and N. H. Dekker. Double-stranded RNA under force and torque: Similarities to and striking differences from double-stranded DNA. *Proc. Natl. Acad. Sci. U. S. A.*, 111(43):15408–15413, 2014.
20. M. L. Bennink, S. H. Leuba, G. H. Leno, J. Zlatanova, B. G. de Grooth, and J. Greve. Unfolding individual nucleosomes by stretching single chromatin fibers with optical tweezers. *Nat. Struct. Biol.*, 8(7):606–610, 2001.
21. G. D. M. Jeffries, J. S. Edgar, J. Zhao, J. P. Shelby, C. Fong, and D. T. Chiu. Using polarization shaped optical vortex traps for single-cell nanosurgery. *Nano Lett.*, 7(2):415–420, 2007.
22. X. Wang, S. Chen, M. Kong, Z. Wang, K. D. Costa, R. A. Li, and D. Sun. Enhanced cell sorting and manipulation with combined optical tweezer and microfluidic chip technologies. *Lab Chip*, 11(21):3656–3662, 2011.
23. Y. Pang, H. Song, J. H. Kim, X. Hou, and W. Cheng. Optical trapping of individual human immunodeficiency viruses in culture fluid reveals heterogeneity with single-molecule resolution. *Nature Nanotech.*, 9(8):624–630, 2014.
24. R. Huang, I. Chavez, K. M. Taute, B. Lukić, S. Jeney, M. G. Raizen, and E.-L. Florin. Direct observation of the full transition from ballistic to diffusive Brownian motion in a liquid. *Nature Phys.*, 7(7):576–580, 2011.
25. Yogesha, S. Bhattacharya, and S. Ananthamurthy. Characterizing the rotation of non symmetric objects in an optical tweezer. *Opt. Commun.*, 285(10–11):2530–2535, 2012.
26. E. Schäffer, S. F. Nørrelykke, and J. Howard. Surface forces and drag coefficients of microspheres near a plane surface measured with optical tweezers. *Langmuir*, 23(7):3654–3665, 2007.
27. A. Yao, M. Tassieri, M. Padgett, and J. Cooper. Microrheology with optical tweezers. *Lab Chip*, 9:2568–2575, 2009.

28. N. Nève, J. K. Lingwood, J. Zimmerman, S. S. Kohles, and D. C. Tretheway. The μPIVOT: an integrated particle image velocimeter and optical tweezers instrument for microenvironment investigations. *Meas. Sci. Technol.*, 19(9):095403, 2008.
29. S. Xu, L. Lou, Y. Li, and Z. Sun. On the aggregation kinetics of two particles trapped in an optical tweezers. *Colloids Surf. A*, 255(1–3):159–163, 2005.
30. C. Probst, A. Grünberger, W. Wiechert, and D. Kohlheyer. Microfluidic growth chambers with optical tweezers for full spatial single-cell control and analysis of evolving microbes. *J. Microbiol. Methods*, 95(3):470–476, 2013.
31. H. Schneckenburger, A. Hendinger, R. Sailer, M. H. Gschwend, W. S. Strauss, M. Bauer, and K. Schütze. Cell viability in optical tweezers: high power red laser diode versus Nd:YAG laser. *J. Biomed. Opt.*, 5(1):40–44, 2000.
32. E. A. Abbondanzieri, J. W. Shaevitz, and S. M. Block. Picocalorimetry of transcription by RNA polymerase. *Biophys. J.*, 89(6):L61–L63, 2005.
33. M. Mahamdeh and E. Schäffer. Optical tweezers with millikelvin precision of temperature-controlled objectives and base-pair resolution. *Opt. Express*, 17(19):17190–17199, 2009.
34. J. P. Mills, L. Qie, M. Dao, C. T. Lim, and S. Suresh. Nonlinear elastic and viscoelastic deformation of the human red blood cell with optical tweezers. *Mech. Chem. Biosyst.*, 1(3):169–180, 2004.
35. A. Rohrbach. Stiffness of optical traps: quantitative agreement between experiment and electromagnetic theory. *Phys. Rev. Lett.*, 95(16):168102, 2005.
36. S. F. Tolić-Nørrelykke, E. Schäffer, J. Howard, F. S. Pavone, F. Jülicher, and H. Flyvbjerg. Calibration of optical tweezers with positional detection in the back focal plane. *Rev. Sci. Instrum.*, 77:103101-1-11, 2006.
37. H. Labit, A. Goldar, G. Guilbaud, C. Douarche, O. Hyrien, and K. Marheineke. A simple and optimized method of producing silanized surfaces for FISH and replication mapping on combed DNA fibers. *Biotechniques*, 45(6):649–658, 2008.
38. J. A. Maroto and F. J. de las Nieves. Theoretical and experimental comparison of the colloid stability of two polystyrene latexes with different sign and value of the surface charge. *Colloid Polym. Sci.*, 276(6):453–458, 1998.
39. Y. Gan. Invited Review Article: A review of techniques for attaching micro- and nanoparticles to a probe's tip for surface force and near-field optical measurements. *Rev. Sci. Instrum.*, 78(8):081101-1-8, 2007.
40. L. A. C. Lüderitz and R. v Klitzing. Interaction forces between silica surfaces in cationic surfactant solutions: An atomic force microscopy study. *J. Colloid Interface Sci.*, 402:19–26, 2013.

41. S. Guo and B. B. Akhremitchev. Packing density and structural heterogeneity of insulin amyloid fibrils measured by AFM nanoindentation. *Biomacromolecules*, 7(5):1630–1636, 2006.

Index